Development of Fatigue Life Prediction Method for Spot-Welded Joints of Mixed Materials

by

Changjian Wei

A thesis submitted in partial fulfillment
of the requirements for the degree of
Master of Science in Engineering
(Mechanical Engineering)
in the University of Michigan-Dearborn
2017

Master's Thesis Committee:

Associate Professor Hong-Tae Kang, Chair
Professor Yi Zhang
Associate Professor German Reyes

ACKNOWLEDGEMENTS

I would first like to express my sincere appreciation and gratitude to my advisor, Associate Professor Hong-Tae Kang, for his support, advice and guidance throughout my study.

I would also like to thank Professor Yi Zhang and Associate Professor German Reyes as my thesis defense committee members, and I am gratefully indebted to them for their very valuable comments on this thesis.

Finally, I must express my very profound gratitude to my parents for providing me with unfailing support and continuous encouragement throughout my years of study and through the process of researching and writing this thesis. This accomplishment would not have been possible without them. Thank you.

TABLE OF CONTENTS

LIST OF FIGURES

LIST OF TABLES

ABSTRACT

Spot-welded joints are widely employed in the construction of vehicle structures. Recently, due to the strategies for minimizing the fuel consumption and vehicle emissions, more and more applications of lightweight materials, such as aluminum (Al) alloys, are employed in spot-welded joints. Hence, a universal and simple fatigue life prediction method is needed for conventional steel spot-welded joints as well as mixed materials spot-welded joints.

In this study, a new notch stress approach is developed for fatigue life evaluation of the spot-welded joint. The idea of this method originates from Rupp's structural stress method, which has been successfully used in automotive industry. The structural stress method is simple enough, but there are nine parameters needed to be adjusted for each new experimental data. Thus, the primary goal of the new approach is to eliminate the troublesome parameters. Stress intensity factors SIFs and stress concentration factors are introduced to solve this issue. Then, having considered the boundary conditions and crack propagation effects, some correction factors are applied to the new notch stress approach in this study. Finally, three groups of spot weld fatigue data including steel, aluminum alloys and their combination are processed with the new notch stress approach for validation. Compared with Rupp's structural stress method, distinct improvements are presented in this study.

CHAPTER I

INTRODUCTION

Spot-welded joints in thin-sheet materials are most common joining method in the structural components of automobiles: car body, chassis components, truck cab, van box. A conventional car body contains several thousands of spot welds. Nowadays they are others joining methods such as riveting, bolting, clinching and bonding that substitute the spot-welded joints to some extent, However, despite those mentioned above competitive joining methods, spot welding will remain important at least for thin-sheet structures in mild or low-alloy steels because it is a cheap and robust joining method.

Spot welding technique is not only applied to similar sheets material joints such as steel alloy, but also in dissimilar sheets materials joints. Due to the strategies for reducing fuel consumption and vehicle emissions, the efforts of designing and manufacturing lightweight vehicles are continuously increasing in today's automotive industry. Lightweight materials such as aluminum (Al) alloy can offer much greater potential of fuel economy than cast iron and traditional steel, the idea of joining aluminum and steel in vehicles' bodies and components become popular. Since about 90% of all cracks occurring in car bodies in service, the evaluation methods of fatigue failures originated from spot-welded are in mainly concerned. Method development projects were repeatedly conducted by industrial users and carried out by

university institutes and research laboratories in cooperation with software suppliers with the aim of making fatigue life predictions for spot-welded and similar lap joints more accurate and reliable.

Our literature survey will review three types of the method in evaluating fatigue behaviors of spot-welded joints.

In the modern design process, the use of calculations and simulations is an essential feature. As described by Fermér and Svensson [1], several properties such as strength, stiffness, durability, handling, ride comfort and crash resistance can today be numerically analyzed with varying levels of accuracy. Development time can be shortened with the help of CAE. The fatigue assessment methods which are related to finite element analysis should be considered with high priority.

Many researchers [5-21] have used structural stress concepts to predict the fatigue life of spot-welded joints. Structural stresses are chosen as fatigue-relevant quantities in S-N curves so that fatigue life can be predicted based on these curves. Since the direct calculation on the basis of a fine-meshed finite element model of the weld spot is too expensive in general for industrial use. A theory which allows calculation of the structural stresses at the weld spot edge from the weld spot forces is needed. In another word, structural stress method is a finite element basis approach, and it is mesh size independent. Note that another reason for determining the structural stress based on the forces and moments at spot welds is that the coarse mesh (in relation to sheet thickness and nugget diameter) of the routine finite element models cannot offer sufficiently accurate local stresses around the spot welds but they can provide rather

accurate forces and moments transferred by the spot welds. [3]

According to Rupp [5], Structural stresses are determined from the resultant internal forces and moments in the joint face of the weld spot (shear forces, cross-tension force and bending moments, the torsional moment being neglected) both in the structural component and in the specimen. For that purpose, simple engineering formulae are available, which are derived using simplifying assumptions with respect to the elastic weld spot behavior. The maximum structural stresses at the weld spot edge are determined either in the plates or in the nugget depending from where the fatigue cracks propagate. They are termed ‘nominal structural stresses' [2]. And nominal structural stress is defined as being linearized over the plate thickness, which consists of membrane stress and pure bending stress.

Structural stress in nCode designlife is based closely upon the work of Rupp and Grubisic [5]. The weld spot resultant forces are determined from the single-bar model by evaluating the forces in the two nodal points of the bar or beam element and the corresponding nodal points of the shell elements connected to them. The load transfer is locally concentrated at the nugget edge, whereas the interior of the weld spot remains more or less stress-free.

The structural stress in nCode is contributed from three parts: membrane stress due to in-plane shear forces, bending stress due to bending moments and bending stress due to opening forces acting perpendicular to the spot weld plane. The first part of structural stress is related to spot weld diameter d and plate thickness t; the remained two parts are not only related to diameter d and thickness t but also depend on the assumed circular plate outer diameter D [6]. Since spot weld nugget in nCode model is described as a rigid inclusion in the center of the

circular plate. However, the ratio of outer diameter D and spot weld diameter d is fixed as 10. In order to narrow the S-N curves scatter band for all kinds of materials, nine parameters are proposed to modified the structural stresses data. These nine parameters, which are mainly determined by experimental data, include diameter exponent, thickness exponent and scaling factor for three parts of structural stress respectively.

The fatigue assessment procedure for spot-welded joints based on structural stresses is well established for industrial use. But it fails to take the eigen-forces in the into account, which may have a significant influence on the service life to be predicted. The importance of the eigen-forces was independently recognized by Sheppard [7,8,9] and Radaj [10,11]. A weak point of the Rupp–Grubisic version of the approach is the fact that only those structural stresses are introduced, which can be attributed to the weld spot resultant forces in the joint face. But there are also structural stresses generated by self-equilibrating forces in each of the two overlapping plates, which are termed ‘eigen-forces.' A more severe problem with the structural stress approach is the fact that the notch effect of the weld spot edge is completely neglected. Battelle researchers have developed a mesh-insensitive nodal force based Battelle structural stress method which has been proven to be highly effective in correlating fatigue behaviors of welded joints [12-17]. Battelle structural stress is developed on an equilibrium equivalent decomposition of an arbitrary through-thickness stress state at the location of interest such as weld toe. Similar to the concept in nCode structural stress, the original Battelle structural stress is also defined as being linearized over the plate thickness, which consists of membrane stress and pure bending stress. However, a new self- equilibrating stress concept was introduced with

the objective of considering the structural stress concentration factor SCF due to the notch effect of weld toe. The stress distribution representing the self-equilibrating part of the stress distributions can be seen as two linear distributions, which equilibrates within itself through thickness [18]. Then, the structural stress is the superposition of original linearized stress and self-equilibrating stress. Another difference between nCode structural stress method and Battelle structural stress method is that crack propagation effect is involved in Battelle structural stress. According to J.K. Hong [19], based on a two-stage crack growth model, an equivalent structural stress parameter has been derived using fracture mechanics principles which have been shown to consolidate all plate joint fatigue data relevant to steel structures onto a narrow band. Since equivalent structural stress parameter has been proven to be highly effective in seam welded structure, it is not difficult to apply the same concept to spot weld if one assume that the spot weld circumferential edge line can be regarded as the seam weld line. Thus, an enormous coordinate matrix is needed for transferring the local coordinate stress to global coordinate stress [20]. In order to simplify the spot weld structural stress calculation procedure, a simplified version for spot weld is proposed [19]. Spot weld is modeled with beam elements which connect two sheets of shell elements without mesh refinements. To calculate the structural stress, the six nodal forces and moments in beam elements are of primary interest. Methodologies for estimating structural stress are based on the work of Rupp et al. [5]. It is worth mentioning that the definition of membrane stress in Battelle structural stress is twice larger than in nCode. Since in Battelle structural stress, the in-plane shear force is assumed to act uniformly over the half of the weld nugget periphery [21].

There are many researchers [22-28] who have used stress intensity factors SIFs as a parameter to predict the fatigue life of spot-welded joints. The stress intensity approach uses the stress intensity factor at the slit tip of spot-welded directly to describe the fatigue strength. It does not include a crack propagation analysis. The maximum value of the cyclic equivalent stress intensity factor at the weld spot edge, i.e. at the slit front, is considered to be the decisive parameter characterizing the fatigue strength and service life of specimens. The equivalent stress intensity factor is determined from the stress intensity factors of the crack opening modes I, II and III according to a relevant strength criterion. There are different strength criterions according to proposals by Irwin [29], Erdogan and Sih [30] or Sih [31].

How to obtain SIFs at the weld spot edge becomes the central issue of developing an SIF basis method. Pook [22,23] has proposed an SIFs method based on nominal stress. In his approach, simple approximative formulae are developed for the stress intensity at the weld spot edge in which the mean shear stress and the weld spot diameter*d* are the dominant parameters. Whereas, according to Radaj [27,28], it is advantageous to transform these mean shear stress to the mean normal stress in the plate and the plate thickness as the dominant parameters for the stress intensity factor. Zhang [3,4] has investigated the relationship between structural stress in the sheet plate and SIFs at spot weld edge based on J-integral. Typical loads of tensile-shear, cross-tension and coach-peel are derived from a number of simple formulas on the basis of an analytic solution. SIFs at spot welds edge under general loading conditions are estimated in terms of the forces and moments transferred by the spot welds based on the derivations. It is worth mentioning that in dissimilar sheet material specimens, SIFs at a small distance ahead of

the spot weld slit crack tip are characterized in a complex from, which is mainly due to the singularity stress field around spot weld crack tip [32]. Pan and Lin [33,34] extended Zhang's work and developed analytic closed-form structural stress and stress intensity factor solutions for spot welds in commonly used specimens by using the equilibrium conditions and classical Kirchhoff plate theory. The specimens' dimensions were considered as an important geometric effect in the SIFs calculation. Also, self-balanced force concept was proposed in their method, which is equivalent to the concept of eigen-force proposed by Radaj [2].

There is a close link between SIFs method and notch stress method since the notch stress is directly related to the stress intensity factors around the crack tip in spot weld joints. Lawrence et al. [35] had given the expression of stress filed ahead of the blunt crack tip (stress field is controlled by SIFs). The tangential stress along the interior surface of a blunt crack tip under mixed modes is the notch stress needed to be determined. By applying the SIFs equations of Pook [22,23], Lawrence developed the notch stress equations for tensile-shear specimen and also provided the expression of relevant elastic stress concentration factors K_t. It should be noted that, according to Neuber [36], the maximum notch stress according to the theory of elasticity is not decisive for crack initiation and propagation but instead some lower local stress gained by averaging the notch stresses over a material characteristic small length at the notch root is critical. Therefore, it is the fatigue effective SCFs K_f should be used instead of K_t in fatigue life evaluation. This can be achieved by some simple formulas which can transfer K_t to K_f by assuming a larger fictitious notch radius. Zhang [3] developed his notch stress equation based on the stress field ahead of the blunt crack tip according to Pook. However, the

SIFs of Zhang's notch stress method is determined by his SIFs solution. Another difference between Zhang's approach and Pook's approach is that Zhang added a non-singular notch stress term in his equation. Similarly, in Radaj's notch stress approach [37], the notch effect of the structural stress which produces no stress singularity at the sharp slit tip is also considered. Furthermore, Radaj believed that the notch stress concentration from mode II loading approximated by the solution of Creager and Paris [38] for a parabolic blunt crack is too low. Therefore, a keyhole shape notch crack tip model was applied in his notch stress approach. Also, the corresponding stress field for finite keyhole shape notch radius was given in his paper in 2001

References

[1] Fermér M and Svensson H,'Industrial experiences of FE-based fatigue life predictions of welded automotive structures', Fatigue Fract Engng Mater Struct, 2001, 24, 489–500.

[2] Radaj D, 'Fatigue Assessment of Welded Joints by Local Approaches' Abington Publishing, Cambridge, UK.

[3] Zhang, S. Stress intensities at spot welds. Int. J. Fract. 1997; 88: 167–185.

[4] Zhang, S. Stress intensities derived from stresses around a spot weld. Int. J. Fract. 1999; 99: 239–257.

[5] Rupp A, Störzel K and Grubisic V, 'Computer-aided dimensioning of spotwelded automotive structures', SAE Techn Paper 950711, Warrendale Pa, SAE, 1995.

[6] Nakahara, Y., Takahashi, M., Kawamoto, A., Fujimoto, M. et al. Method of Fatigue Life Estimation for Spot-Welded Structures SAE 2000-01-0779

[7] Sheppard S D, 'Estimation of fatigue propagation life in resistance spot welds', Advances in Fatigue Lifetime Predictive Techniques, Vol 2, ASTM STP 1211, Philadelphia Pa, ASTM, 1993, pp 169–185.

[8] Sheppard S D, 'Further refinement of a methodology for fatigue life estimation in resistance spot weld connections', Advances in Fatigue Lifetime Predictive Techniques, Vol 3, ASTM STP 1292, Philadelphia Pa, ASTM, 1996.

[9] Sheppard S D and Strange M, 'Fatigue life estimation in resistance spot welds: initiation and early growth phase', Fatigue Fract Engng Mater Struct, 1992, 15 (6), 531–549.

[10] Radaj D, 'Vollständige Bestimmung der Kräfte am Schweißpunkt', Ing-Archiv, 1990, 60, 389–398.

[11] Radaj D, 'Theory of forces and stresses in spot-welded overlap joints', Archive Appl Mech, 1996, 67, 2–34.

[12] Dong, P., Hong, J.K., and Cao, Z., A Mesh-Insensitive Structural Stress Procedure for Fatigue Evaluation of Welded Structures, IIW Doc. XIII-1902-01/XV-1089-01, 2001.

[13] Dong, P., Hong, J. K., Osage, D.A., and Prager, M., 'Master S-N Curve Method for Fatigue Evaluation of Welded Components,' Welding Research Council Bulletin 474, Welding Research Council, 2002.

[14] Dong, P., Hong, J.K., and Cao, Z., 'Structural Stress Based Master S-N Curve for Welded Joints,' IIW Doc. XIII-1930-02/XV-1119-02, 2002.

[15] Dong, P. and Hong, J.K., 'The Master S-N Curve Approach to Fatigue of Vessel and Piping Welds,' Welding in the World 48(1/2): 28-36, 2003.

[16] Dong, P. and Hong, J. K., 'The Master S-N Curve Approach to Fatigue Evaluation of Offshore and Marine Structures,' in the Proceedings of the OMAE 2004, Volume 2, OMAE2004-51324, 2004.

[17] Dong, P., Hong, J. K., and De Jesus, A. M. P., 'Analysis of Recent Fatigue Data Using the Structural Stress Procedure in ASME Div 2 Rewrite,' Transactions of ASME, Journal of Pressure Vessel Technology 139(3): 355-362, 2007.

[18] Dong, P., Hong, J.K., and Cao, Z., 'Stresses and stress intensities at notches: anomalous crack growth revisited', International Journal of Fatigue 25 (2003) 811–825

[19] Hong, J.K. Battelle. The development of a simplified spot weld model for Battelle structural stress calculation. SAE Technical Paper, 2011-01-0479

[20] Kang H, Dong, P., Hong, J.K. 'Fatigue analysis of spot welds using a mesh-insensitive structural stress approach', International Journal of Fatigue 29 (2007) 1546–1553

[21] Maddox, S. J., 'Fatigue Design of Welded Structures,' Engineering Design in Welded Constructions, Pergamon, Oxford, 31-56, 1992

[22] Pook L P, Approximate stress intensity factors for spot and similar welds, NEL Rep 588, Glasgow, National Engineering Laboratory, 1975.

[23] Pook L P, 'Fracture mechanics analysis of the fatigue behaviour of spot welds', Int J Fract, 1975, 11 (2), 173–176.

[24] Yuuki R and Ohira T, 'Fracture mechanics analysis of the fatigue strength of various spot-welded joints', Seisan Kenyu, 1986, 38 (10), 475–478.

[25] Cooper J F and Smith R A, 'Initial fatigue crack growth at spot welds', Proceedings Conference on Fatigue of Engng Materials and Structures, London, Institute of Mechanical Engineering, 1986, Vol 2, pp 283–288.

[26] Smith R A and Cooper J F, 'Theoretical predictions of the fatigue life of shear spot welds', Fatigue of Welded Constructions, Abington, TWI, 1988, pp 287–295.

[27] Radaj D, ‘Local fatigue-strength characteristic values for spot-welded joints’, Engng Fract Mech, 1990, 37 (1), 245–250, and Schweißen u Schneiden, 1990, 42 (1)

[28] Radaj D, ‘Structural stress, notch stress and stress intensity factor approach for assessment of fatigue-strength of spot-welded joints’, Welding in the World, 1990, 28, 29–39.

[29] Irwin G R, ‘Analysis of stresses and strains near the end of a crack traversing a plate’, Trans ASME, J Appl Mech, 1957, 24, 361–364.

[30] Erdogan F and Sih G C, ‘On the crack extension in plates under plane loading and transverse shear’, Trans ASME, J Basic Engng, 1963, 85, 519–527.

[31] Sih G C, ‘A three-dimensional strain energy density factor theory of crack propagation’, Three-dimensional Crack Problems, Leyden, Noordhoff, 1975, pp 15–80.

[32] Rice, J.R. and Sih, G.C. (1965). Plane problems of cracks in dissimilar media. Journal of Applied Mechanics 32, 418–423.

[33] Lin, P.-C., Pan, J., 2008a. Closed-form structural stress and stress intensity factor solutions for spot welds in commonly used specimens. Engineering Fracture Mechanics, 45 (2008) 3996–4020

[34] Lin, P.-C., Pan, J. Closed-form structural stress and stress intensity factor solutions for spot welds under various types of loading conditions, International Journal of Solids and Structures 45 (2008) 3996–4020

[35] Lawrence, F.V., Wang, P.C. and Corten, H.T. (1983). An Empirical Method for Estimating the Fatigue Resistance of Tensile-Shear Spot Welds, SAE Paper 830035.

[36] Neuber H (1968) Über die Berücksichtigung der Spannungskonzentration bei Festigkeitsberechnungen. Konstruktion 20:245–251

[37] Radaj D, Lehrke H P and Greuling S, ‘Theoretical fatigue-effective notch stresses at spot welds’, Fatigue Fract Engng Mater Struct, 2001, 24, 293–308.

[38] Tada, H., Paris, P. and Irwin, G. (1985). The Stress Analysis of Cracks Handbook, Paris Productions Incorporated and Del Research Corporation.

CHAPTER II

FATIGUE TEST RESULTS AND FAILURE OBSERVATION OF SPOT WELD JOINTS

2.1. Introduction

This Chapter mainly presents the fatigue test results of spot-welded joints. Historical fatigue data are included for comparison. The specimens can be classified into three group according to the sheets materials: steel to steel, aluminum (Al) alloys to aluminum alloys and mixed combination of steel to aluminum alloys. For each group, there are two types of specimen geometry: tensile-shear (TS) and coach-peel (CP). A special case of double spot welds joints was designed in steel to steel specimens, whereas historical steel to steel and other materials fatigue data group only had single spot weld joint specimens. All the fatigue results are displayed in load range versus life to failure plots.

2.2. Fatigue test results of steel to steel specimens

2.2.1 Double spot-welded joint

In the steel to steel double spot-welded joint group, different sheet thickness combinations and the average of spot weld diameters are listed in Table 2.1. The specimen configuration and the details of dimension are shown in Fig 2.1.

Table 2.1. Steel to steel double spot weld dimensions

Material 1	Material 2	LS Button Diameter (mm)	CP Button Diameter (mm)
1.2 mm DP600	1.2 mm DP600	4.60	4.60
0.65 mm DP600	0.65 mm DP601	4.60	4.38
0.65 HSLA340	0.65 HSLA340	4.60	4.60
0.65 HSLA341	1.2 mm DP600	4.60	4.68
1.2 mm HSLA340	1.2 mm HSLA340	4.78	4.60

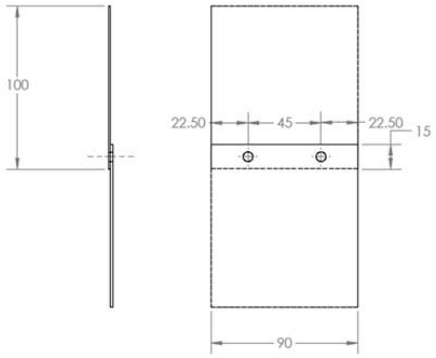

Specimen dimensions in mm

(a) Tensile-Shear

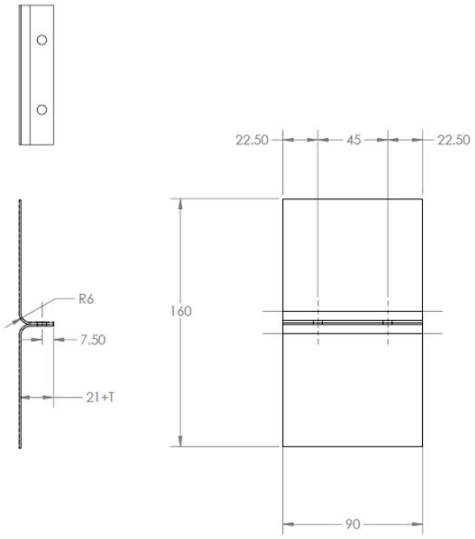

Specimen dimensions in mm

(b) Coach-Peel

Figure 2.1. Steel to steel double spot weld configuration

A load ratio (R) of 0.1 was carried out for all fatigue tests. The fatigue results are displayed in load range versus life to failure plots as Fig 2.2 shown. In TS case, specimens with larger sheet thickness have longer fatigue life. However, the material effect of different steel is less significant. CP specimens share the similar feature as TS, but thickness has more significant effect in the joints fatigue life. Note that the L-N curve of CP has a greater gradient than TS.

2.2.1 Single spot-welded joint

Historical fatigue data from A/SP [1] for steel to steel single spot weld were used in this study for comparison. The specimen details are listed in Table 2.2, and the specimen configuration is shown in Fig 2.3. Then, all the steel to steel fatigue data of load range versus life cycles to failure is plotted on the same graph as shown in Fig 2.4.

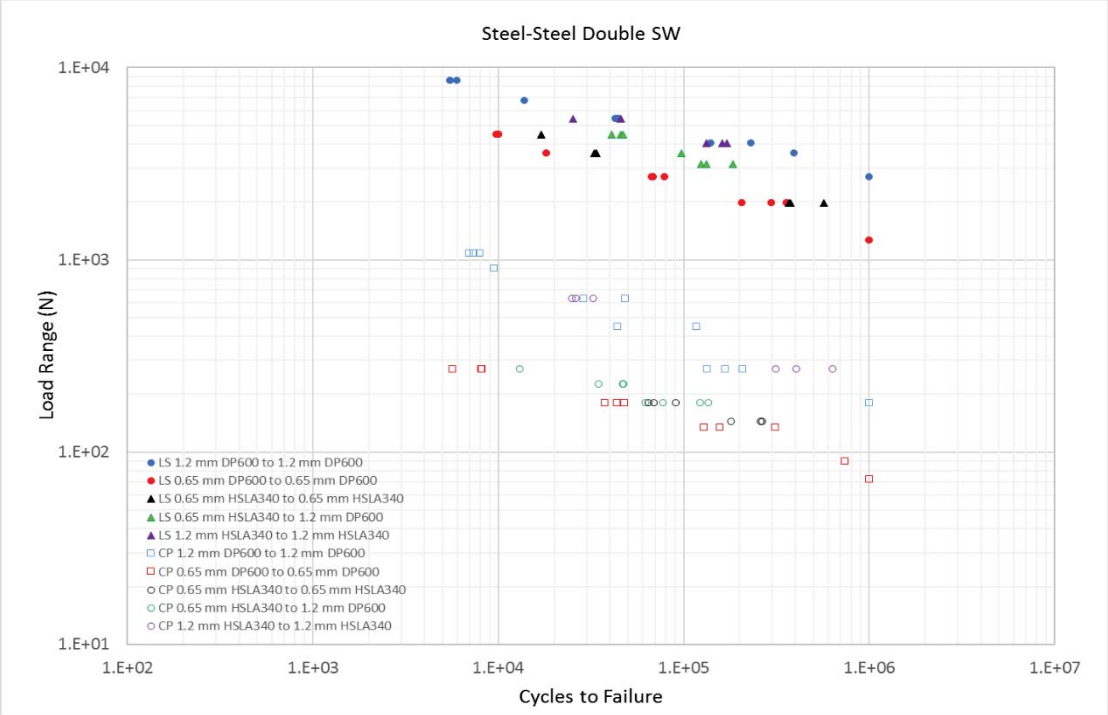

Figure 2.2. Load range versus cycles to failure diagram for steel-steel double SW

Table 2.2 Steel to steel single spot weld dimensions

Material 1	Material 2	LS Button Diameter (mm)	CP Button Diameter (mm)
1.5mm DP600	1.5mm DP600	7	7
1.6mm DP800	1.6mm DP800	7	7
1.6mm DQSK	1.6mm DQSK	7	7
1.5mm HSLA340	1.5mm HSLA340	7	7
1.6mm IF	1.6mm IF	7	7
1.6mm MS1300	1.6mm MS1300	7	7
1.39mm RA830	1.39mm RA830	7	7
1.5mm TRIP600	1.5mm TRIP600	7	7

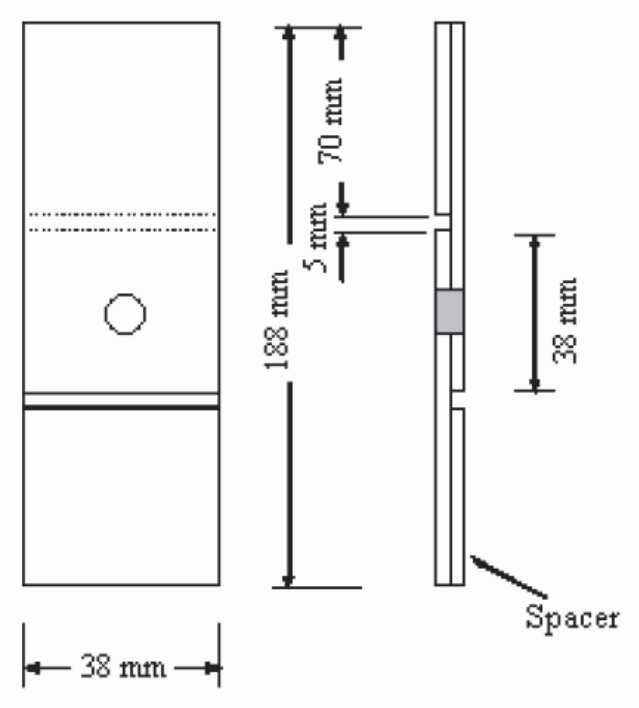

(a) Tensile-Shear

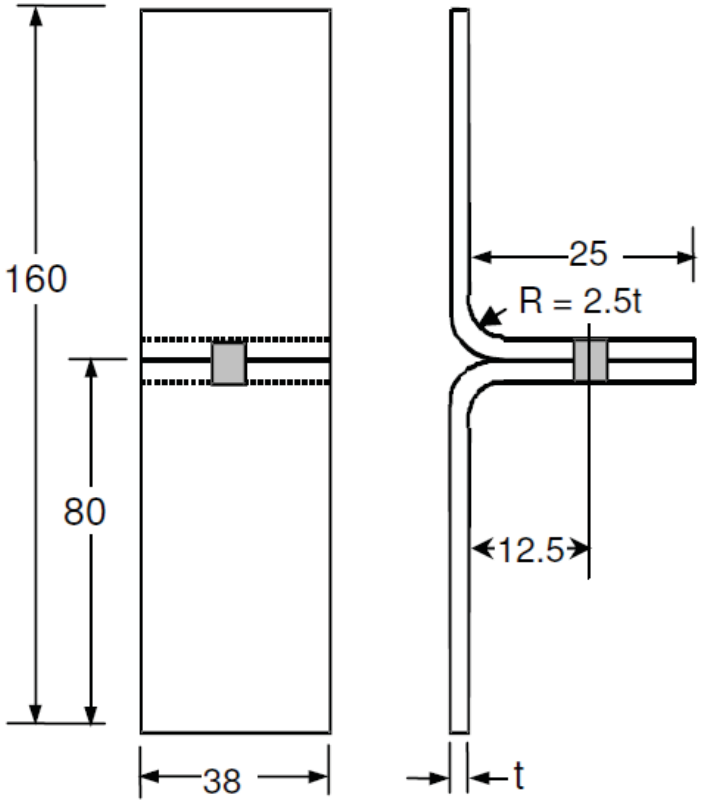

(b) Coach Peel

Figure 2.3. Steel to steel single spot weld configuration

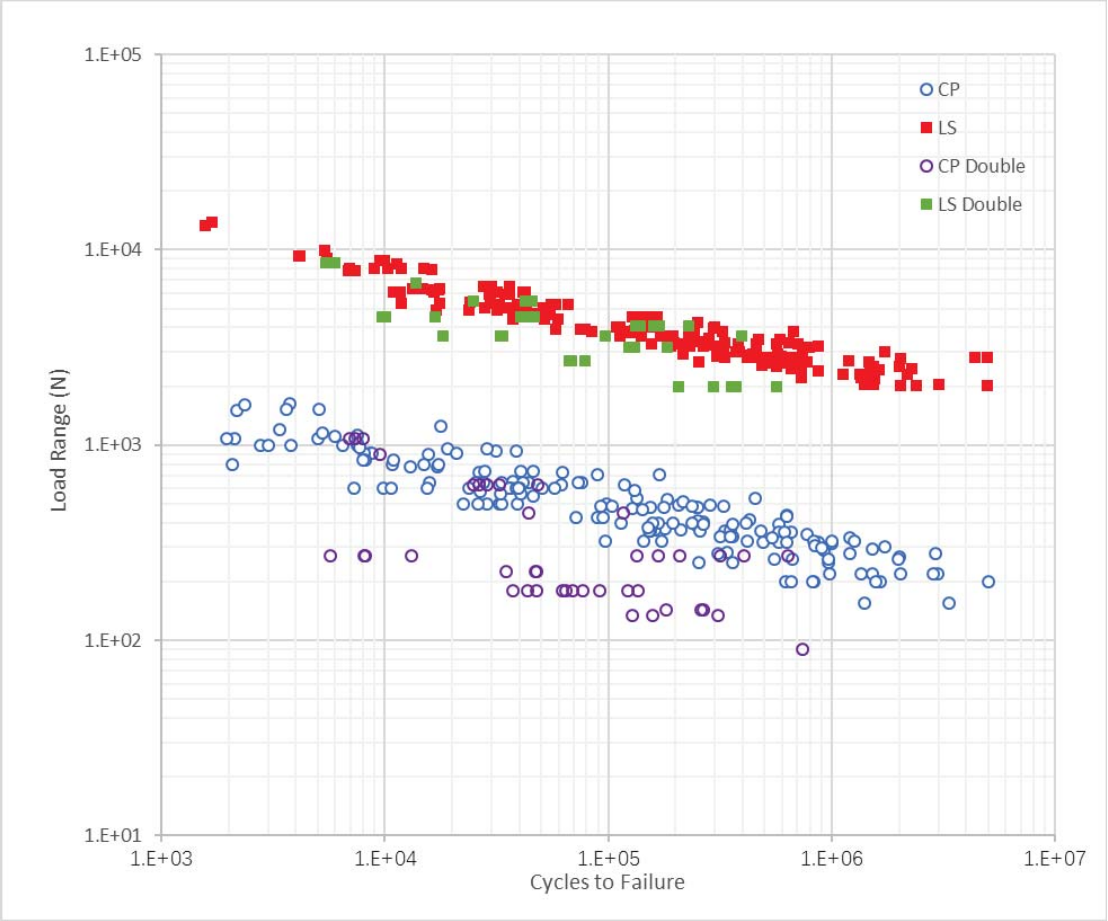

Figure 2.4. Load range versus cycles to failure diagram for steel-steel

Figure 2.5. Typical failure mode of steel-steel SW

Most of the single and double spot weld specimen fail at plate sheet which can be classified into two types as Fig 2.5 shows: button pull and eye-brow. Button pull failure commonly occurs in low cycles fatigue, whereas eye-brow failure happens in high cycles fatigue.

2.3. Fatigue test results of Al to Al specimens

In the aluminum (Al) alloys to aluminum alloys spot weld group, different sheet thickness combinations and the average of spot weld diameters are listed in Table 2.3. The specimen configuration is the same as steel to steel single spot weld, which has been shown in Fig 2.3.

Table 2.3. Al to Al single spot weld dimensions

Material 1	Material 2	LS Button Diameter (mm)	CP Button Diameter (mm)
1.1mm 5182 O3	1.1mm 5182 O3	5.67	5.76
2.4mm 5754 O	2.4mm 5182 O	8.09	7.99
1.2mm X611 T4PD	1.2mm X611 T4PD	5.96	5.80
2.0mm 7003.30-T5	2.0mm 7003.30-T5	8.39	-
1.2mm X611 T4PD	1.2mm 5754 O	6.03	-

The load range versus cycles to failure plot is presented in Fig 2.6, similar fatigue features are revealed compared to steel to steel spot weld group. There is a difference in failure mode between these two groups of the spot weld. In thin sheet specimen of which thickness $t \leq 1.2\text{mm}$, most of the cracks propagate through sheet thickness which happens in both two groups. Whereas in thicker sheet CP specimen (2.4mm X611 T4PD aluminum alloy), interfacial failure of spot weld nugget is the dominant failure mode. Fig 2.7 (a) shows the typical interfacial failure mode of thick sheet CP specimen and (b) shows the typical button pull failure mode of thin sheet CP specimen.

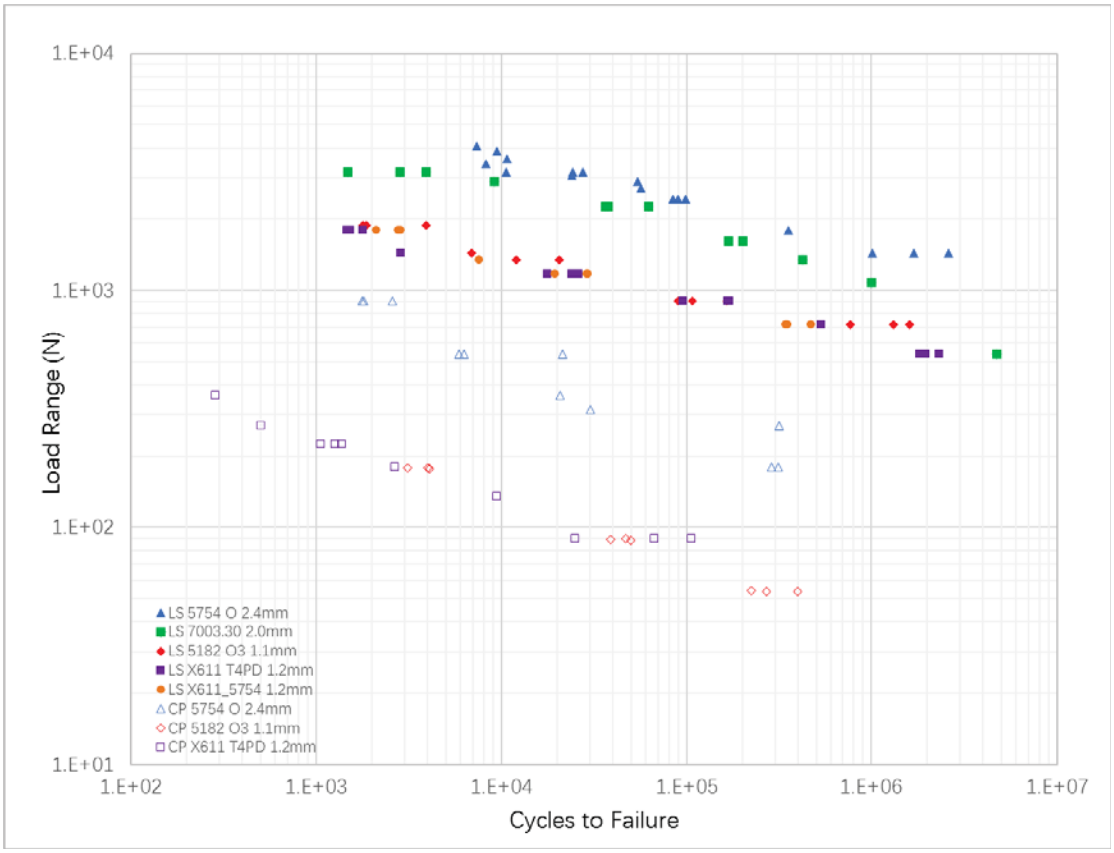

Figure 2.6. Load range versus cycles to failure diagram for Al-Al

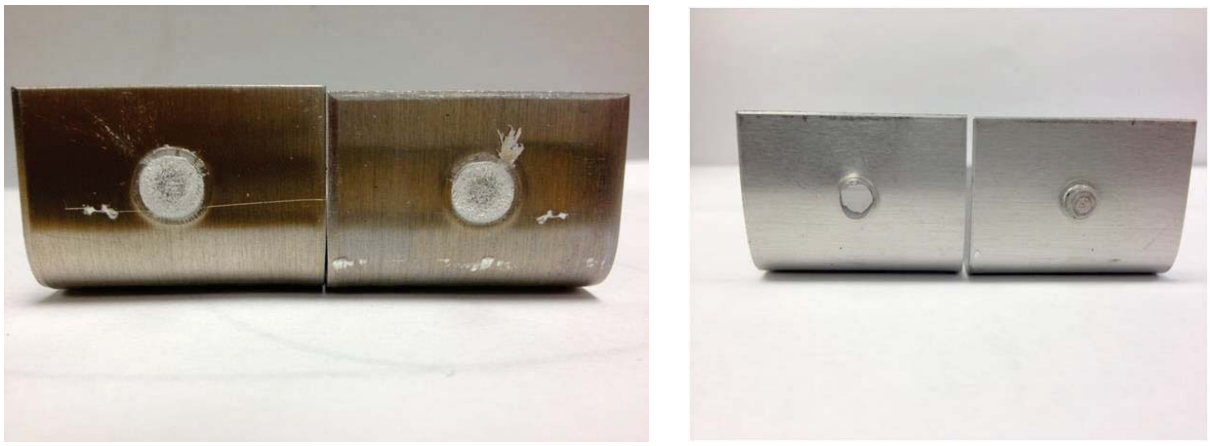

(a)Interfacial failure (b)Button pull failure

Figure 2.7. Typical failure mode of Al-Al SW

2.4. Fatigue test results of Al to Steel specimens

In the Al to steel mixed materials spot-welded joint group, different sheet thickness combinations and the average of spot weld diameters are listed in Table 2.4. The specimen

configuration and the details of dimension are shown in Fig 2.8.

Table 2.4. Al to steel spot weld dimensions

Material 1	Material 2	LS Button Diameter (mm)	CP Button Diameter (mm)
0.8mm x626	0.9mm HDG LCS	4.9	6.5
0.8mm x626	1.2mm HDG LCS	4.7	6.1
1.2mm 6022	1.2mm HDG LCS	4.2	6.1
1.2mm 6022	1.2mm HSLA	4.2	7.3

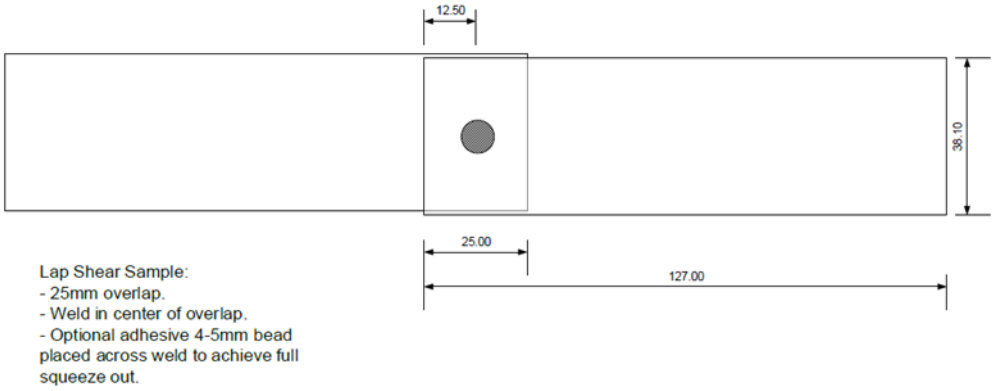

(a) Tensile-shear

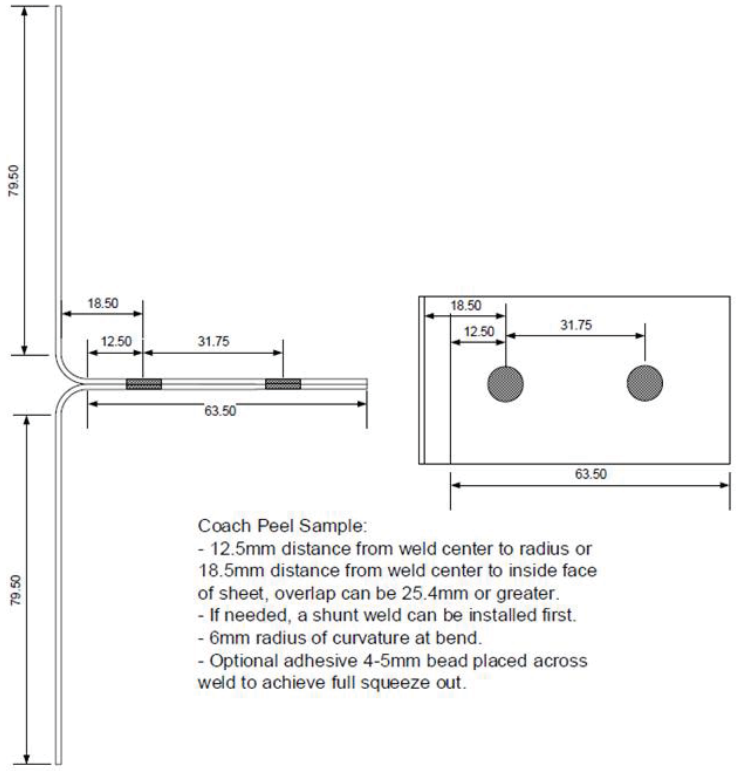

(b) Coach-Peel

Figure 2.8. Al to steel spot weld configuration

The load range versus cycles to failure plot is shown in Fig 2.9. The L-N curves for both TS and CP are flatter than other two groups of fatigue data. Even the thickness variation is quite small (for Al sheet, from 0.8mm to 1.2mm), there is a distinct separation between different sheet thickness specimens, especially for CP.

The fatigue failure happens in Al sheet, and the failure modes are similar to steel to steel case, which is that button pull failure commonly occurs in low cycles fatigue and eye-brow failure happens in high cycles fatigue.

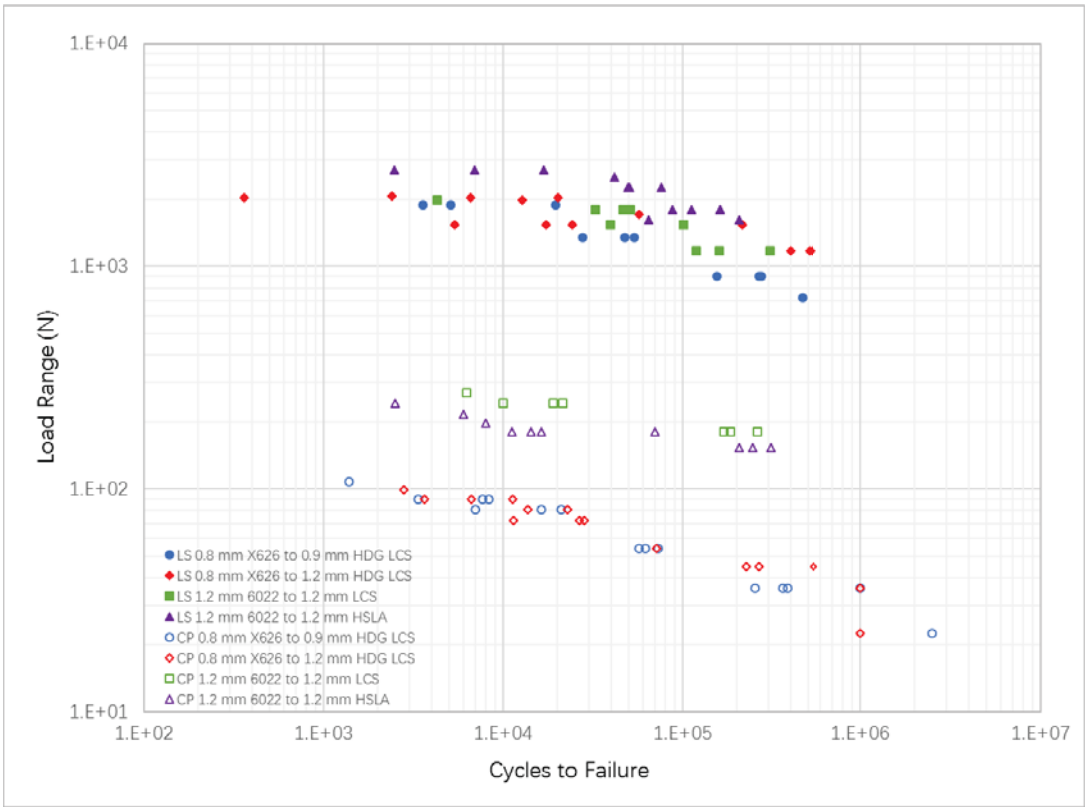

Figure 2.9. Load range versus cycles to failure diagram for Al-steel

References

[1] Bonnen, J., Agrawal, H., Amaya, M., Iyengar, R. et al., "Fatigue of Advanced High Strength Steel Spot-Welds," SAE Technical Paper 2006-01-0978

CHAPTER III

THEORY OF NOTCH STRESS APPROACH IN SPOT WELDED JOINTS

3.1. Introduction

This chapter mainly presents the principles and procedure of the notch stress approach with regard to spot-welded joints. Stress intensity factor (SIF) approach is reviewed and organized, since there is a close link between the stress intensity and notch stress.

In the past, numerous investigations have attempted to determine the structural stress of spot welds for fatigue life prediction based on S-N curve. However, a severe problem with the structural stress approach is the fact that the notch effect of the weld spot edge is completely neglected (it varies with the local loading condition). The limitation is revealed to some extent by the necessity to use structure-related instead of material-related S–N curves.

The notch stress approach is also based on S-N curve method to predict fatigue life, however, instead of using structural stress, a new parameter notch stress need to be determined. Note that the notch stress is based on the initiation stage of the crack, which means that the effect of through-thickness crack propagation is not considered in notch stress analysis. There are two ways of defining the shape and size of the notch at the weld spot edge, either close to the real cross-sectional micro shape of the slit tip, avoiding any unrealistic undercut, or as a

substitute notch with a pronounced undercut (i.e. keyhole notch). The U-shape notch proposed by Pan and Sheppard [3] and also by Zhang and Richter [4] or the semielliptical notch applied for comparison by Seeger et al. [5] enforces an extremely small notch radius in gapless joints (radius equal to surface roughness). The parabolic notch proposed by Lawrence et al.967 significantly underestimates the notch effect in mode II loading. The keyhole notch in gapless joints proposed by Radaj et al. [6] notch in gaping joints may represent worst case conditions with the restriction that the undercut is more effective in mode II than in mode I loading. The size of the keyhole notch should be as small as possible in order to keep the cross-sectional weakening effect low. A notch radius of r = 0.05 mm is recommended in low-carbon steels. In this study, a simple sharp crack tip is defined as the shape of the notch of the spot weld, which avoids any undercut effect, and a size of notch radius r=0.05mm is used in notch stress calculation. The detail of the notch shape and size will be discussed in section 3.3.

The stress concentration factors SCFs are the key to relating structural stress (or nominal stress) with notch stress. However, SCFs cannot be readily determined by the local geometry of spot weld. Then, stress intensity factors SIFs are required to established the connection between structural stress and notch stress, since notch stress around crack tip is controlled by the SIFs and SIFs can be determined by the structural stress distribution in the sheets using simple engineering formulas. The following sections will reveal the detail procedure of notch stress calculation.

In section 3.2, the relationship between structural stress and SIFs is presented. Two typical essential specimens tensile-shear and coach peel are demonstrated as examples. In

section 3.3, the relationship between SIFs and SCFs is discussed in a more general loading condition. In section 3.4, the boundary condition and geometric effect are considered, and some correction parameters are required for spot weld in a real structure. Finally, section 3.5 presents the result of notch stress approach in the application of specimens.

3.2. The relationship between structural stresses and SIFs

3.2.1. Decomposition of structural stresses in different plate thickness

The singular part of the stress state at the slit tip is described by singular terms characterized by the stress intensity factors KI (normal tension), KII (in-plane shearing) and KIII (out-of-plane shearing). We define as pure mode I, II and III states the self-equilibrating loading states with the external forces acting in the same line in the opposite direction along the two sides of the slit face. These loading states are characterized by the fact that the external forces are equilibrated entirely by themselves. The forces act completely around the slit tip line (the slit front) producing the stress singularity there. However, non-self-equilibrating forces would provide reaction forces at the external supports which are attributable to the non-singular state. The stress which causes no stress singularity at the tip usually will be separated from the total structural stress, so that the remained portion can be used to calculate the stress intensity factor.

Consider a general case of unequal plate thicknesses but similar material. The stress

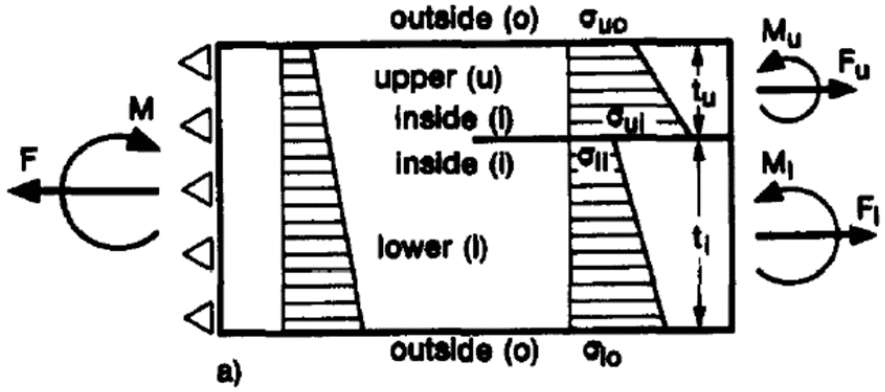

Figure 3.1. Stress distributions around a spot-welded joint

distributions of the spot-welded joint in a sheet specimen can be expressed on the radial cross section plane through the center line of the spot weld nugget based on Radaj and Zhang's plane contour model [7], which is shown in Figure 3.1. In this model, two sheets of similar materials jointed by spot weld are analyzed. The sheet on the top is called the "upper sheet" and abbreviated by "u" which would be shown as the subscripts of other terms. The sheet at the bottom is called the "lower sheet" and abbreviated by "l" for the subscripts of other terms. Additionally, the inner surface between two sheets, including the lower surface of the top sheet and the upper surface of the bottom sheet, is abbreviated by "i" for subscripts, whereas the outer surface of both sheets, including the upper surface of the top sheet and the lower surface of the bottom sheet, is abbreviated by "o" for subscripts. The four normal stresses σ_{ui}, σ_{uo}, σ_{li}, σ_{lo} indicate the linearly distributed structural stresses at the inner (i) or outer (o) surface of the upper (u) or lower (l) sheet. Note that the shear stresses distribution is neglected and only dominate normal stresses are considered in this study. Since we treated the spot weld nugget as a rigid cylindrical inclusion and expressed the 3-dimensional stress distributions in a 2-dimensional radial cross-section plane, the normal stresses σ_u, σ_l indicate the linearly distributed structural stresses through two sheet plates.

In the first step, stress which does not cause a stress singularity is separated. The non-singularity support stresses, which are distributed within spot weld nugget and characterized by σ_u, σ_l, are determined by support forces, F and M, which are deduced from the equilibrium conditions:

$$F = F_u + F_l \tag{3.1}$$

$$M = M_u + M_l - F_u \frac{t_l}{2} + F_l \frac{t_u}{2} \tag{3.2}$$

According to above equation:

$$\sigma_l = \frac{\sigma_{lo} t_l^2 + \sigma_{ui} t_u^2 + (2\sigma_{li} + 2\sigma_{lo} - \sigma_{ui} - \sigma_{uo}) t_u t_l}{(t_u + t_l)^2} \tag{3.3}$$

$$\sigma_u = \frac{\sigma_{uo} t_u^2 + \sigma_{li} t_l^2 + (2\sigma_{ui} + 2\sigma_{uo} - \sigma_{li} - \sigma_{lo}) t_u t_l}{(t_u + t_l)^2} \tag{3.4}$$

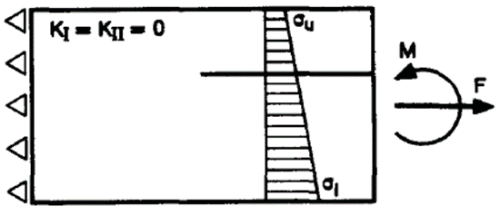

Figure 3.2. Non-singularity stress distributions

After subtraction of the non-singularity stresses, the remaining stresses are:

$$\sigma'_{uo} = \sigma_{uo} - \sigma_u \tag{3.5}$$

$$\sigma'_{ui} = \sigma_{ui} - \frac{\sigma_u t_l + \sigma_l t_u}{t_u + t_l} \tag{3.6}$$

$$\sigma'_{li} = \sigma_{li} - \frac{\sigma_u t_l + \sigma_l t_u}{t_u + t_l} \tag{3.7}$$

$$\sigma'_{lo} = \sigma_{lo} - \sigma_l \tag{3.8}$$

These stresses are separated according to the self-equilibrating load cases, tension-bending, and counter bending:

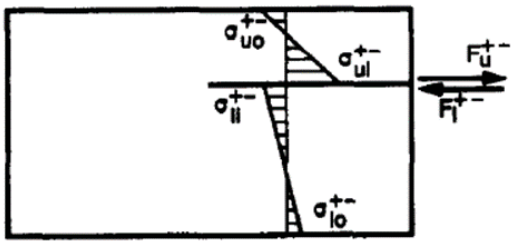

Figure 3.3. Tension-bending load case

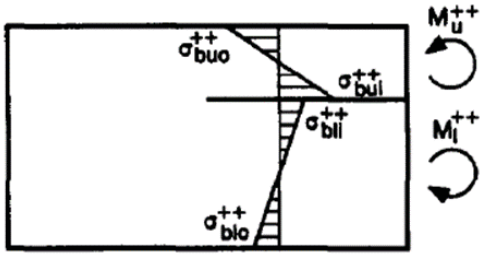

Figure 3.4. Counter bending load case

In a more general decomposition, tension-bending can be separated into in-plane shear and central bending. Stress from these two loading models will be contributed to the stress intensity factor K_{II}. However, in counter bending case, stress will be contributed to the stress intensity factor K_I.

3.2.2. Decomposition of structural stresses in equal thickness

To simplify the stress equation, the special case of equal plate thickness is considered. The different plate thickness spot-welded joint can be regarded as the equal thickness of the thinner plate in the analysis for simplicity.

In this model, two sheets of similar materials and equal plate thickness of spot-welded joint are analyzed. The structural stress distributed in the sheet can be decomposed into four type of stress: “Symmetrical membrane," "Anti-symmetrical membrane," "Symmetrical bending” and “Anti-symmetrical bending," as Fig 3.5 shown.

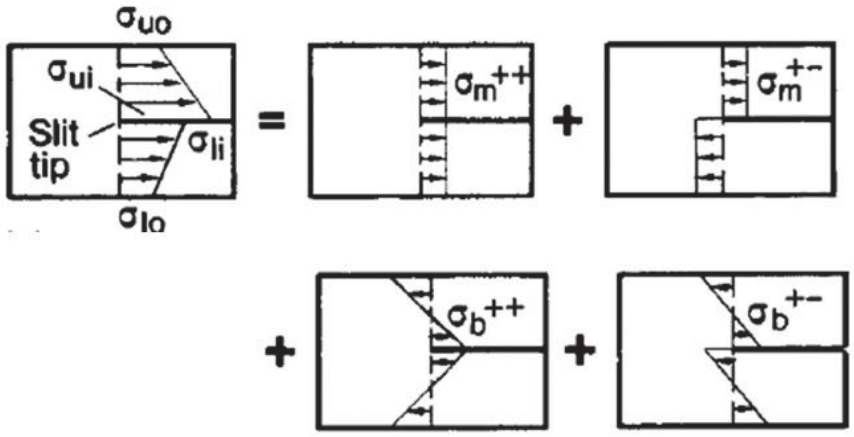

Figure 3.5. Decomposition of structural stresses in equal thickness

Here, a stress is termed symmetrical (++), if it has the same value and sign (or direction) at corresponding points above and below the slit tip. For antisymmetrical stress (+-), the sign is reversed.

The symmetrical membrane stress is corresponding to the non-singularity stress in different thickness case since symmetrical membrane has no contribution in SIFs. The anti-symmetrical membrane stress combined with anti-symmetrical bending stress are corresponding to the tension-bending as mentioned previously, these two types of stress cause mode II damage to the crack tip. Similarly, the symmetrical bending stress is corresponding to the counter bending stress, which causes mode I damage to the crack tip.

3.2.3. SIFs solutions under various types of loading conditions

Before the derivation of SIFs on the basis of structural stress, a presupposition should be clear. The weld spot diameter is large in relation to the plate thickness or at least greater than the plate thickness. The stress singularities at opposite slit tips are mutually influenced if the

slit tips come closer together.

Once the structural stresses along the rigid inclusion circumference are decomposed into four types of the loading conditions, the strip model of Radaj and Zhang [8] can then be adopted to derive approximate stress intensity factor solutions for spot welds Fig. 3.6 shows a two-dimensional model of two infinite strips with connection under plane strain conditions. The two strips have the same thickness t. As schematically shown in Fig. 3.6, the stress intensity factors can then be determined from the structural stress distributions and the J-integral based on the strip model.

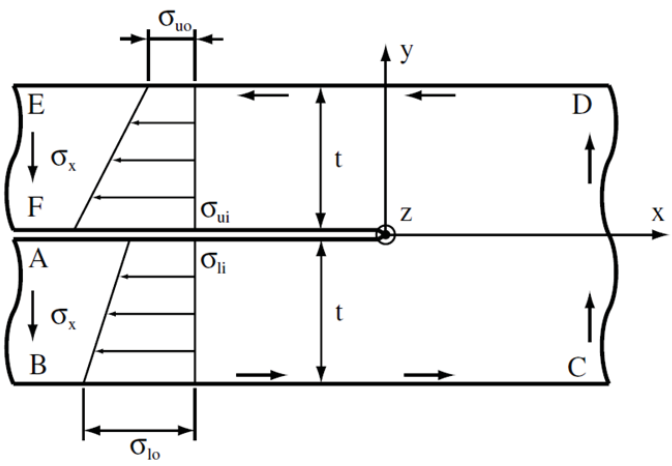

Figure 3.6. The front and side views of the left half of the strip model.

For linear elastic materials, the J-integral (Rice, 1968) represents the energy release rate. Under plane strain conditions, the J-integral is related to K_I, K_{II} as:

$$J = \frac{1-v^2}{E}(K_I^2 + K_{II}^2) \tag{3.9}$$

Radaj and Zhang [7,8] defined the J-integral for this model as:

$$J = \int_{\Gamma} \left(W n_x - T_i \frac{\partial u_i}{\partial x}\right) ds \tag{3.10}$$

where Γ is the integration contour for the J-integral calculation and W is the strain energy density, which is given as:

$$W = \frac{1}{2}\left(\sigma_x \varepsilon_x + \sigma_y \varepsilon_y + \tau_{xy}\gamma_{xy}\right) \tag{3.11}$$

As Figure 3.6 shows, the selected counterclockwise contour ABCDEFG around the initial crack point on a Cartesian coordinate system. The initial crack point is chosen to be the origin of coordinate. Here, σ_x and σ_y are the normal stress in the x-direction and y-direction, respectively. ε_x and ε_y are the normal strain in the x-direction and y-direction, respectively. τ_{xy} and γ_{xy} are shear stress and shear strain on the xy-plane, respectively. The integrals along line BC and line DE are zero because n_x is zero and T_i are zeros. For the integrals along line AB, line CD and line EF, the contributions of the shear stress τ_{xy} are taken to be zero in Radaj and Zhang [8]. Therefore, we can simply the Equation (3.10) and Equation (3.11) as:

$$J = -\left(\int_{\overline{AB}} W dy + \int_{\overline{CD}} W dy + \int_{\overline{EF}} W dy\right) \tag{3.12}$$

$$W = \frac{1}{2}(\sigma_x \varepsilon_x) = \frac{1-\nu^2}{E}\sigma_x^2 \tag{3.13}$$

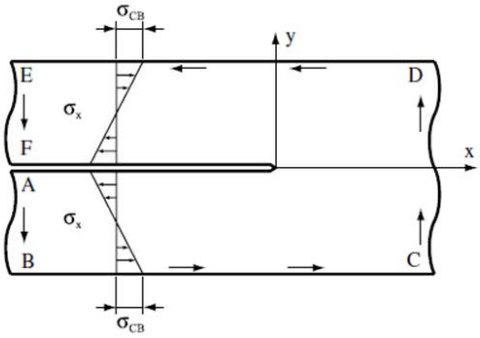

Figure 3.7. Counter bending (symmetrical bending) model.

Since the integrals along line BC and line DE are zero, line AB, line CD and line EF can be taken near the crack tip or at the far ends of the infinite strips by the path independence of the J-integral.

First, consider the case under counter bending load condition (symmetrical bending). As schematically shown in Fig. 3.7, the structural stresses σ_{CB} have no contribution to K_{II}

and K_{III} . The integral along line CD is zero because line CD is traction free due to the self-equilibrating loading conditions of counter bending. Based on the classical Kirchhoff plate theory, the normal stress σ_x along line AB can be defined as:

$$\sigma_x = \sigma_{CB}(1 + \frac{2y}{t}) \tag{3.14}$$

Similarly, the normal stress σ_x along line EF can be defined as:

$$\sigma_x = \sigma_{CB}(1 - \frac{2y}{t}) \tag{3.15}$$

Combining Eqs. (3.12), (3.14) and (3.15) gives the J-integral as:

$$J = \frac{-(1-v^2)}{2E}\{\int_0^{-t}\left[\sigma_{CB}\left(1+\frac{2y}{t}\right)\right]^2 dy + \int_t^0\left[\sigma_{CB}\left(1-\frac{2y}{t}\right)\right]^2 dy = \frac{\sigma_{CB}^2 t(1-v^2)}{3E} \tag{3.16}$$

Since $K_{II} = 0,\ K_I$ solution for symmetrical bending is:

$$K_I = \frac{\sigma_{CB}\sqrt{t}}{\sqrt{3}} \tag{3.17}$$

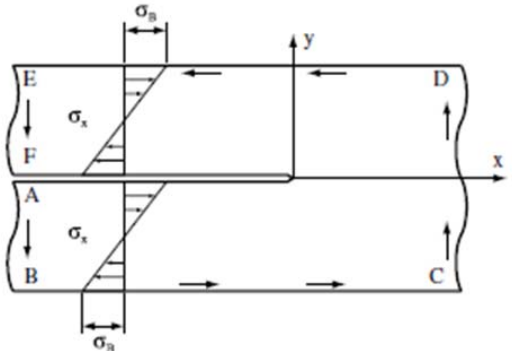

Figure 3.8. Central bending (anti-symmetrical bending) model.

Then, consider the case under central bending loading condition (anti-symmetrical bending). As schematically shown in Fig. 3.8, the structural stresses have no contribution to K_I. For central bending, the derivations of the integrals are similar to those for counter bending. However, an additional bending moment along line CD is required in order to balance the two bending moments along line AB and line EF. Based on the classical Kirchhoff plate theory, the

normal stress along line AB can be defined as:

$$\sigma_x = -\sigma_B(1 + \frac{2y}{t}) \tag{3.18}$$

Similarly, the normal stress σ_x along line EF can be defined as:

$$\sigma_x = \sigma_B(1 - \frac{2y}{t}) \tag{3.19}$$

The normal stress σ_x along line CD can be defined as:

$$\sigma_x = -\frac{\sigma_B y}{2t} \tag{3.20}$$

Combining Eqs. (3.12), (3.18), (3.19) and (3.20) gives the J-integral as:

$$J = \frac{-(1-v^2)}{2E}\{\int_0^{-t}[\sigma_B\left(1+\frac{2y}{t}\right)]^2 dy + \int_{-t}^{t}\left(\frac{-\sigma_B y}{2t}\right)^2 dy \int_t^0 [\sigma_B\left(1-\frac{2y}{t}\right)]^2 dy = \frac{\sigma_B^2 t(1-v^2)}{4E} \tag{3.21}$$

Since $K_I = 0$, K_{II} solution for anti-symmetrical bending is:

$$K_{II} = \frac{\sigma_B\sqrt{t}}{2} \tag{3.22}$$

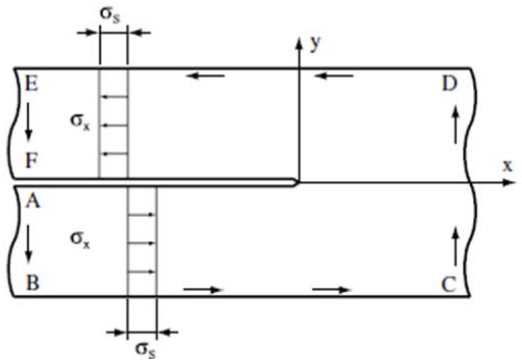

Figure 3.9. In-plane shear (anti-symmetrical membrane) model

Finally, consider the case of anti-symmetrical membrane loading condition. As schematically shown in Fig. 3.9, The structural stresses have no contribution to K_I. An additional bending moment along line CD is required in order to balance the moment due to the shear forces along line AB and line EF. The detailed derivations of the integrals for the K_{II}

solution is similar to those for anti-symmetrical bending and are not repeated here. The J-integral for anti-symmetrical membrane can be written as:

$$J = -\left(\int_{\overline{AB}} W dy + \int_{\overline{CD}} W dy + \int_{\overline{EF}} W dy\right) = \frac{\sigma_s^2 t(1-v^2)}{4E} \tag{3.23}$$

Since $K_I = 0,\ K_{II}$ solution for the anti-symmetrical membrane is:

$$K_{II} = \frac{\sigma_s \sqrt{t}}{2} \tag{3.24}$$

3.2.4. SIFs solutions application to tensile-shear specimen

According to the works of Radaj [7] and Radaj and Zhang [9], loads of various types of specimens containing spot welds can be decomposed into several symmetric and anti-symmetric parts based on the superposition principle of the linear elasticity theory. One typical basic specimen tensile-shear is analyzed. Fig 3.10. schematically shows the decomposition of the shear load of the central part of a tensile-shear specimen. Based on the schematic of the lap-shear specimen shown in Fig 3.10, schematics of the symmetry cross sections near the spot welds under various types of loads are shown as model A–F. In these schematics, two strips of sheets with the thickness t represent the upper and lower sheets and the gray area with a size of d = 2a represent the spot weld. Model A represents a spot weld under lap-shear loading conditions. The shear forces F represent the resultant forces applied to the ends of the sheets along the interfacial surface of the nugget. Model B represents a spot weld under an equivalent loading condition of model A. As shown in the figure, the shear forces F are shifted from the plane of the interfacial surface of the nugget to the middle surface of the upper and lower sheets. Two additional bending moments Ft/2 are required for equilibrium. Finally, the forces and moments of model B are decomposed into four types of simple loads: symmetrical bending,

anti-symmetrical bending, anti-symmetrical membrane and symmetrical membrane, indicated as models C, D, E, and F, respectively. The bending moment in model C and D has a magnitude of Ft/4, and the force in model E and F has a magnitude of F/2.

According to the previous discussion in section 3.2.2, model F symmetrical membrane has no contribution in SIFs. Based on section 3.2.3, SIFs in model C, D and E can be calculated by structural stress distributed in plates. And the structural stress can be easily obtained from forces and moments acting on the sheet plates. First, consider model E, which is under anti-symmetrical membrane loading condition. The resultant force acting on the spot weld nugget is F/2+F/2=F. And the anti-symmetrical membrane stress (nominal structural stress) in the plate from loading the core or weld spot by the force F in the plate plane is the maximum radial membrane stress in the plate at the core edge, which can be determined as:

$$\sigma_m^{+-} = \frac{F}{\pi dt} \tag{3.25}$$

According to Eqs. (3.24), the SIFs solution is:

$$K_{II} = \frac{F}{2\pi d\sqrt{t}} \tag{3.26}$$

Then, consider model D, which is under anti-symmetrical bending loading condition. The resultant moment acting on the spot weld nugget is Ft/4+Ft/4=Ft/2. And the anti-symmetrical bending stress (nominal structural stress) from loading the core or weld spot by the bending moment $\mathrm{M} = \mathrm{Ft}/2$ in the plate plane is the maximum radial bending stress x in the plate at the core edge, which can be determined as:

$$\sigma_b^{+-} = \frac{6}{\pi}\frac{(Ft/2)}{dt^2} \tag{3.27}$$

According to Eqs. (3.22), the SIFs solution is:

$$K_{II} = \frac{3}{\pi}\frac{(Ft/2)\sqrt{t}}{dt^2} \tag{3.28}$$

Finally, consider model C, which is under symmetrical bending loading condition. The resultant moment acting on the spot weld nugget is Ft/4-Ft/4=0, which means that the moments acting on the two sides of the plates cancel each other and cannot be captured by the spot weld nugget nodal moment in FEM. This type of force/moment is defined as self-balanced force/moment. However, symmetrical bending stress is still existed within sheet plate and can be determined as:

$$\sigma_b^{++} = \frac{6}{\pi}\frac{(Ft/4)}{dt^2} \tag{3.29}$$

According to Eqs. (3.17), the SIFs solution is:

$$K_I = \frac{2\sqrt{3}}{\pi}\frac{(Ft/4)\sqrt{t}}{dt^2} \tag{3.30}$$

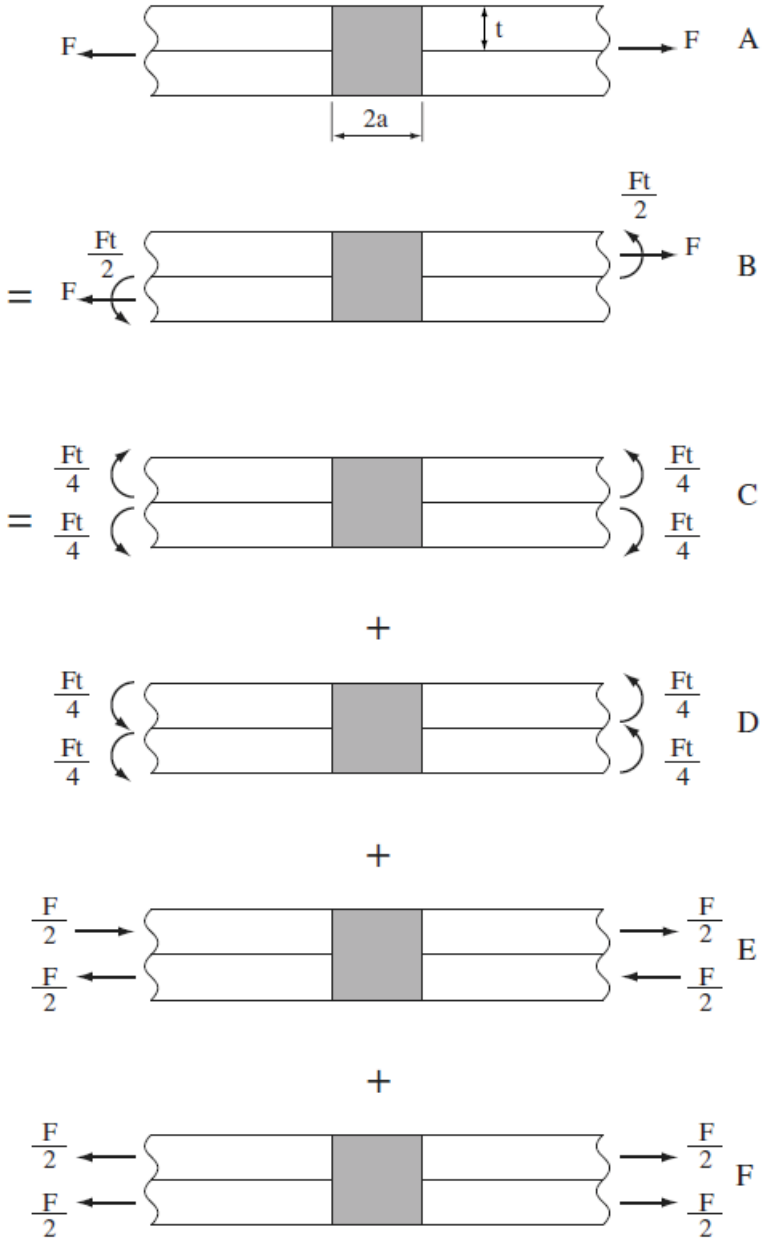

Figure 3.10. Decomposition of tensile-shear specimen

3.2.5. SIFs solutions application to coach peel specimen

Another typical basic specimen coach peel is analyzed. Fig 3.11. schematically shows the decomposition of the peeling load of a coach peel specimen. Based on the schematic of the coach peel specimen shown in Fig 3.11, schematics of the symmetry cross sections near the spot welds under various types of loads are shown as model A−C. Model A represents a spot

weld under coach peel loading conditions. The peeling forces F represent the resultant forces applied to the ends of the sheets. Model B and C combined represents a spot weld under an equivalent loading condition of model A. As shown in the figure, the forces F are shifted from the edge of the sheet to the centroid of the spot weld nugget, which is the opening force F_z in model C, and a pair of additional pure counter bending moments M are added to spot weld nugget.

First, consider model B, which is under symmetrical bending loading condition. The resultant moment acting on the spot weld nugget is M, and the symmetrical bending stress can be determined as:

$$\sigma_b^{++} = \frac{6M}{\pi d t^2} \tag{3.31}$$

According to Eqs. (3.17), the SIFs solution is:

$$K_I = \frac{2\sqrt{3}M}{\pi d t\sqrt{t}} \tag{3.32}$$

Then, consider model C, which is also under symmetrical bending loading condition. Note that the opening force causes a counter bending moment that can be regarded as $M = F_z \cdot d/2$. Then similar to model B, the symmetrical bending stress can be determined as:

$$\sigma_b^{++} = \frac{6F_z \cdot d/2}{\pi d t^2} = \frac{3F_z}{\pi t^2} \tag{3.31}$$

According to Eqs. (3.17), the SIFs solution is:

$$K_I = \frac{\sqrt{3}}{\pi}\frac{F_z\sqrt{t}}{t^2} \tag{3.32}$$

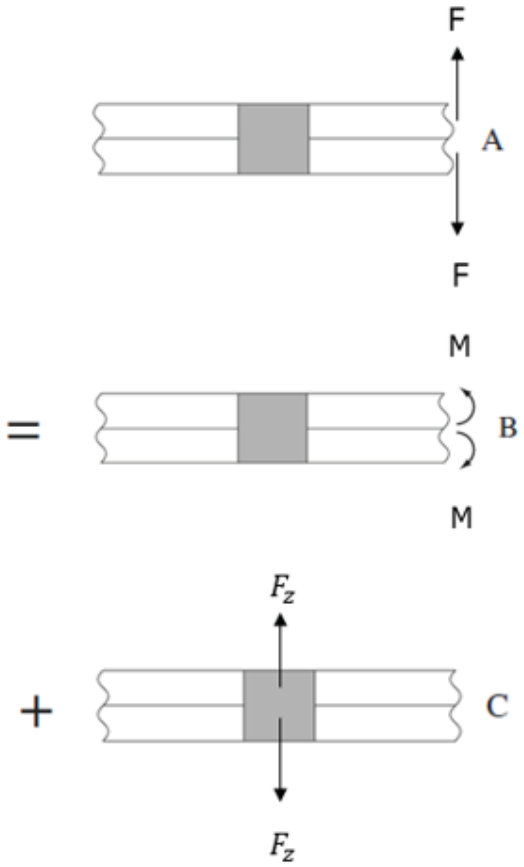

Figure 3.11. Decomposition of coach peel specimen.

3.3. The relationship between SIFs and SCFs

3.3.1. SIFs under mixed mode loading conditions

The slit tips of a spot weld in a vehicle structure are exposed to mixed mode loading conditions. some sort of equivalent stress intensity factor is needed. Before the derivation of equivalent SIF K_{eq}, an assumption should be claimed: the stress intensity factors at spot welds under general loading conditions in the real structures can be constituted by superposing the stress intensities derived for the tensile-shear and coach-peel spot welds. Once above

assumption is established, it can be further induced by the fact that general loading conditions in the real structures can be constituted by superposing the loading for the tensile-shear and coach-peel spot welds.

According to Erdogan and Sih [10], Eqs (3.33) and (3.34) have been successfully used for spot welds by Yuuki et al. [11]

$$K_{eq} = K_I \cos^3\left(\frac{\theta_{max}}{2}\right) - 3K_{II}\cos^2\left(\frac{\theta_{max}}{2}\right)\sin\left(\frac{\theta_{max}}{2}\right) \tag{3.33}$$

$$\theta_{max} = 2\,\mathrm{atan}\left(\frac{1}{4}\left(\gamma - \sqrt{\gamma^2+8}\right)\right),\ \gamma = \frac{K_I}{K_{II}} \tag{3.34}$$

If we define a polar coordinate axis with the origin at the crack tip, the tangential stress and shear stress can be expressed in the polar coordinate system as:

$$\sigma_\theta = \frac{1}{\sqrt{2\pi r}}\left[K_I\cos^3\frac{\theta}{2} - 3K_{II}\cos^2\frac{\theta}{2}\sin\frac{\theta}{2}\right] \tag{3.35}$$

$$\tau_{r\theta} = \frac{1}{\sqrt{2\pi r}}\left[K_I\cos^2\frac{\theta}{2}\sin\frac{\theta}{2} - K_{II}\cos\frac{\theta}{2}(3\cos^2\frac{\theta}{2} - 2)\right] \tag{3.36}$$

When shear stress $\tau_{r\theta} = 0$, the tangential stress σ_θ reaches the maximum value. Compare Eqs (3.33) and (3.35), it is easy to find out that $\sigma_{\theta max}$ is related with K_{eq} and the stress near the crack tip varies with $1/\sqrt{2\pi r}$. If the notch radius ρ is defined, then an equivalent notch stress σ_{eq} can be determined based on the maximum tangential stress:

$$\sigma_{eq} = \frac{K_{eq}}{\sqrt{2\pi\rho}} = \frac{1}{\sqrt{2\pi\rho}}\left[K_I\cos^3\left(\frac{\theta_{max}}{2}\right) - 3K_{II}\cos^2\left(\frac{\theta_{max}}{2}\right)\sin\left(\frac{\theta_{max}}{2}\right)\right] \tag{3.37}$$

Since the crack tip shape like keyhole will change the stress field of the crack tip (Radaj [16] had given the keyhole shape notch stress filed solution based on Airy stress function) and make it too complicated, to simplify the maximum tangential stress equation, a simple sharp tip notch model is used. Therefore, the relationship between equivalent notch stress and equivalent SIF in Eq (3.35) is valid.

3.3.2. Stress concentration factor $\boldsymbol{K_t^m}$

Stress concentration factors SCFs can be defined as the ratio of equivalent notch stress and nominal stress or structural stress:

$$K_t = \frac{\sigma_{eq}}{\sigma_n} \tag{3.38}$$

In the case of membrane only, SIF K_{II} is due to the anti-symmetrical membrane:

$$K_{II} = \frac{F}{2\pi d\sqrt{t}} \tag{3.39}$$

Since there is no K_I, the corresponding equivalent notch stress is:

$$\sigma_{eq}^m = \frac{-3K_{II}\cos^2\left(\frac{\theta}{2}\right)\sin\left(\frac{\theta}{2}\right)}{\sqrt{2\pi\rho}} \tag{3.40}$$

θ depends on the ratio of K_I and K_{II}, according to Eq (3.34), it is easy to obtained $\theta = -70.5°$. The structural stress for the membrane is given by Eq (3.25), and SCF for the membrane is:

$$K_t^m = \frac{\sigma_{eq}^m}{\sigma_n^m} \approx 0.23\sqrt{\frac{t}{\rho}} \tag{3.41}$$

3.3.3. Stress concentration factor $\boldsymbol{K_t^z}$

In the case of bending due to F_z, SIF K_I is due to the symmetrical bending:

$$K_I = \frac{\sqrt{3}}{\pi}\frac{F_z\sqrt{t}}{t^2} \tag{3.42}$$

Since there is no K_{II}, the corresponding equivalent notch stress is:

$$\sigma_{eq}^z = \frac{K_I\cos^3\left(\frac{\theta}{2}\right)}{\sqrt{2\pi\rho}} \tag{3.43}$$

θ depends on the ratio of K_I and K_{II}, according to Eq (3.34), it is easy to obtained $\theta = 0$. The structural stress for bending is given by Eq (3.31), and SCF for bending due to F_z is:

$$K_t^z = \frac{\sigma_{eq}^z}{\sigma_n^z} \approx 0.23\sqrt{\frac{t}{\rho}} \tag{3.44}$$

3.3.4. Stress concentration factor $\boldsymbol{K_t^m}$

In the case of bending due to moment M, it should be emphasized that some portion of the moment is symmetrical bending and rest of the moment is anti-symmetrical bending. According to the assumption that the general loading condition can be constituted by superposing the loading for the tensile-shear and coach peel, the anti-symmetrical bending stress can be related to the nodal shear force F, and the SIF is given by Eq (3.28). Similarly, the self-balanced symmetrical bending stress is also associated with the nodal shear force F, and the SIF is given by Eq (3.28). Once the anti-symmetrical bending portion is determined, the rest of symmetrical bending can be obtained by just subtracting the moment Ft/2 from M. And the symmetrical bending stress is defined as:

$$\sigma_b^{++} = \frac{6}{\pi}\frac{\left(M-\frac{Ft}{2}\right)}{dt^2} \tag{3.45}$$

The corresponding SIF is:

$$K_I = \frac{2\sqrt{3}}{\pi}\frac{\left(M-\frac{Ft}{2}\right)\sqrt{t}}{dt^2} \tag{3.46}$$

Note that M is captured by FEM as the nodal moment acting on the spot weld nugget, the self-balanced moment is not involved in Eq (3.46).

In order to distinguish the stress derived from self-balanced force/moment and stress derived from FEM output nodal force/moment, a superscript “Self” is used to represent self-balanced force/moment type of stress and SIF, Eq (3.30) is upgraded as:

$$K_I^{Self} = \frac{2\sqrt{3}}{\pi}\frac{(Ft/4)\sqrt{t}}{dt^2} \tag{3.47}$$

Similarly, a superscript “N” is used to represent nodal force/moment type of stress and SIF, Eqs (3.28) and (3.46) are upgraded as:

$$K_{II}^{N} = \frac{3}{\pi}\frac{(Ft/2)\sqrt{t}}{dt^2} \tag{3.48}$$

$$K_{I}^{N} = \frac{2\sqrt{3}}{\pi}\frac{\left(M-\frac{Ft}{2}\right)\sqrt{t}}{dt^2} \tag{3.49}$$

Then, combine Eqs (3.37), (3.47), (3.48) and (3.49), the corresponding equivalent notch stress is:

$$\sigma_{eq}^{b} = \frac{K_I^N \cos^3\left(\frac{\theta}{2}\right) - 3K_{II}^N \cos^2\left(\frac{\theta}{2}\right)\sin\left(\frac{\theta}{2}\right)}{\sqrt{2\pi\rho}} + \frac{K_I^{Self}\cos^3\left(\frac{\theta}{2}\right)}{\sqrt{2\pi\rho}} \tag{3.50}$$

Note that the first term of σ_{eq}^{b} is defined as σ_{eq}^{b-N}, which means that the stress is derived from nodal forces/moments, and the second term of σ_{eq}^{b} is defined as σ_{eq}^{b-Self}, which means that the stress is derived from self-balanced forces/moments. θ depends on the ratio of K_I, K_{II}. Here, K_I should be:

$$K_I = K_I^N + K_I^{Self} \tag{3.51}$$

Finally, the structural stress for bending is given by Eq (3.31) and SCF for bending due to moment M:

$$K_t^b = \frac{\sigma_{eq}^b}{\sigma_n^b} \tag{3.52}$$

3.4. The three-dimensional model corrections

3.4.1. Boundary condition

In the previous sections, all the stresses and SIFs were deducted based on two-dimensional strips model. However, a three-dimensional model was more appropriated for spot weld in a real structure. In nCode Designlife, spot weld nugget was described as a rigid inclusion in the center of the circular plate. The outer diameter of the circular plate D was much

larger than the spot weld diameter d. According to Rupp et al. [12], a fixed value D/d=10 was chosen. However, in this study, the ratio of outer diameter and spot weld diameter is an

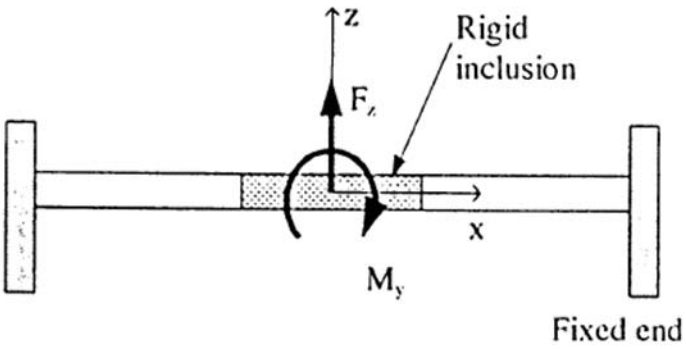

Figure 3.12. Fixed edge boundary condition

adjustable parameter which depends on the real dimensions of the specimens.

The outer edge of the circular plate was assumed to be under fixed support condition in nCode Designlife [12]. Under such boundary condition, according to Nakahara, Y., Takahashi, M., Kawamoto, A., Fujimoto, M. et al. [13], the radial stress along the edge of spot weld nugget should be the structural stress of two-dimensional model multiplied by the correction factors C_m, C_B and C_Z for membrane, pure bending due to moment M and bending due to opening force F_z, respectively. C_B and C_Z are given by:

$$C_B = \frac{1-\left(\frac{d}{D}\right)^2}{1+\left(\frac{d}{D}\right)^2} \tag{3.53}$$

$$C_Z = \frac{\ln\left(\frac{D}{d}\right)}{1-\left(\frac{d}{D}\right)^2} - \frac{1}{2} \tag{3.54}$$

Membrane stress was not affected by the ratio of $\mathrm{D/d}$, therefore, $C_m = 1$.

Since the equivalent notch stress is calculated based on the structural stress of two-dimensional model, the same correction factors C_m, C_B and C_Z are applicable for transferring σ_{eq} to three-dimensional notch stress σ_k. Then the corresponding membrane,

bending due to M and bending due to F_z notch stresses are:

$$\sigma_k^m = \sigma_{eq}^m \tag{3.55}$$

$$\sigma_k^{b-N} = \sigma_{eq}^{b-N} \cdot C_B \tag{3.56}$$

$$\sigma_k^z = \sigma_{eq}^z \cdot C_z \tag{3.57}$$

Note that Eq (3.56) only valid for the stress derived from nodal forces/moments which will be captured by FEM. This is the reason for separating the equivalent notch stress σ_{eq}^b into σ_{eq}^{b-N} and σ_{eq}^{b-Self}. The correction factor for self-balanced equivalent notch stress will be discussed in next section 3.4.2.

3.4.2. Geometric effect on self-balanced forces/moments

In the section 3.2.4, Radaj and Zhang [7,9] had investigated the self-balanced forces/moments in tensile-shear specimens two-dimensional model. Only the self-balanced symmetrical bending moment had the contribution in SIF, which was given by Eq (3.47). And the corresponding equivalent notch stress σ_{eq}^{b-Self} was the second term in Eq (3.50). In order to transfer σ_{eq}^{b-Self} into three-dimensional model notch stress σ_k^{b-Self}, a correction factor similar to C_B need to be determined:

$$\sigma_k^{b-Self} = \sigma_{eq}^{b-self} \cdot C_B^{Self} \tag{3.58}$$

According to P. C. Lin, J. Pan [14], SIFs solutions of tensile-shear's self-balanced moment based on three-dimensional model had given. There were two versions of SIFs solution. The first version was based on the finite square plate model and the second one was based on infinite plate model. The finite square plate assumption was more realistic than an infinite plate, but led to much more complex calculation in SIFs. Therefore, in this study, the

second infinite plate model was selected. In Lin and Pan's model, the self-balanced moments were assumed to be evenly distributed along the edge of the plate. It can be regarded as a model of an infinite plate with a rigid inclusion subjected to a remote uniform counter bending moment $\widetilde{M} = \frac{M}{D} = \frac{Ft/4}{D}$. Here D should be interpreted as the effective diameter of the specimen overlapping region. Then, the line moment acting on the edge of the spot weld nugget at the critical location:

$$\widetilde{M_r} = \frac{F(3+v)}{4D(1-v^2)} \tag{3.59}$$

The corresponding structural stress:

$$\sigma_r = \frac{6\widetilde{M_r}}{t^2} \tag{3.60}$$

And the corresponding SIF:

$$K_I^{bself} = \frac{\sqrt{3}F(3+v)}{4D(1-v^2)\sqrt{t}} \tag{3.61}$$

Then, the correction parameter C_B^{Self} can be determined by the ratio of SIFs solution in Eqs (3.61) and (3.47):

$$C_B^{Self} = 11.4\frac{d}{D} \tag{3.62}$$

Note that the Poisson ratio v in Eq (3.61) is 0.3. Based on Eq (3.62), the correction factor for self-balanced moments also depends on the ratio of $\mathrm{D/d}$.

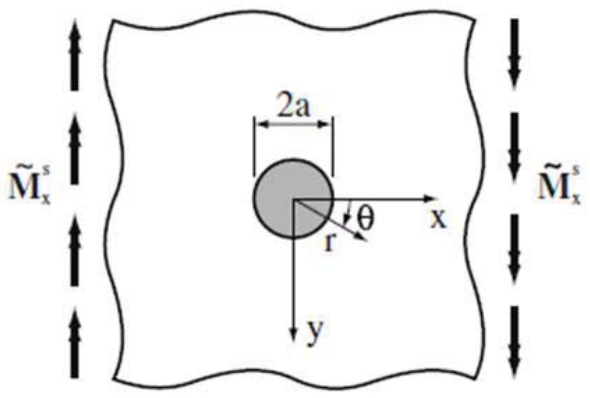

Figure 3.13. Remote uniform self-balanced moment on the plate lateral surface

After considering the boundary conditions and geometric effects on self-balanced forces/moments, the stress concentration factors SCFs should be upgraded as:

$$K_t^m = \frac{\sigma_{eq}^m}{\sigma_n^m} \tag{3.63}$$

$$K_t^b = \frac{\sigma_{eq}^{b-N} \cdot C_B + \sigma_{eq}^{b-Self} \cdot C_B^{Self}}{\sigma_n^b} \tag{3.64}$$

$$K_t^z = \frac{\sigma_{eq}^z}{\sigma_n^z} \cdot C_z \tag{3.65}$$

And the notch stress is defined as:

$$\sigma_k = K_t^m \frac{F}{\pi dt} + K_t^b \cdot \frac{6M}{\pi dt^2} + K_t^z \cdot \frac{3F_z}{\pi t^2} \tag{3.66}$$

It's worth mentioning that K_t^m, K_t^b, K_t^z are the functions of $(\frac{D}{d}, \sqrt{\frac{t}{\rho}})$. This means that the stress concentration factors SCFs are strongly associated with specimen overlapping region's dimension, the spot weld nugget diameter, the sheet thickness and the notch radius. Among them, the nugget diameter d and the sheet thickness t can be measured before the fatigue test. But the notch radius is hard to detected without cutting through the specimen. Therefore, to simplify the procedures of measurement before testing, a typical value of spot-welded joint crack tip radius should be chosen for all the specimens. According to Radaj [1], a notch radius of $\rho = 0.05\text{mm}$ was recommended in low-carbon steels. In this study, ρ is selected to be 0.05mm as a fixed value. As for the effective diameter D, the value should depend on the dimensions of specimen's overlapping region. Since in most of the case, the shape of overlapping region is rectangle, the effective diameter D is defined as the square root of the product of two lengths.

3.5. Applications of notch stress approach

3.5.1. Steel to steel combination for spot-welded joints

As we had mentioned in Chapter II, there were two groups of spot weld specimens fatigue data of steel to steel material combination. One group was the double spot welds specimens with tensile-shear and coach peel and the other group was A/SP single spot weld data in 2005. In order to illustrate the improvement of notch stress method, a comparison to the nCode structural stress method should be made. First, two group of fatigue data were processed with nCode Designlife software. The result is shown in Fig. 3.14.

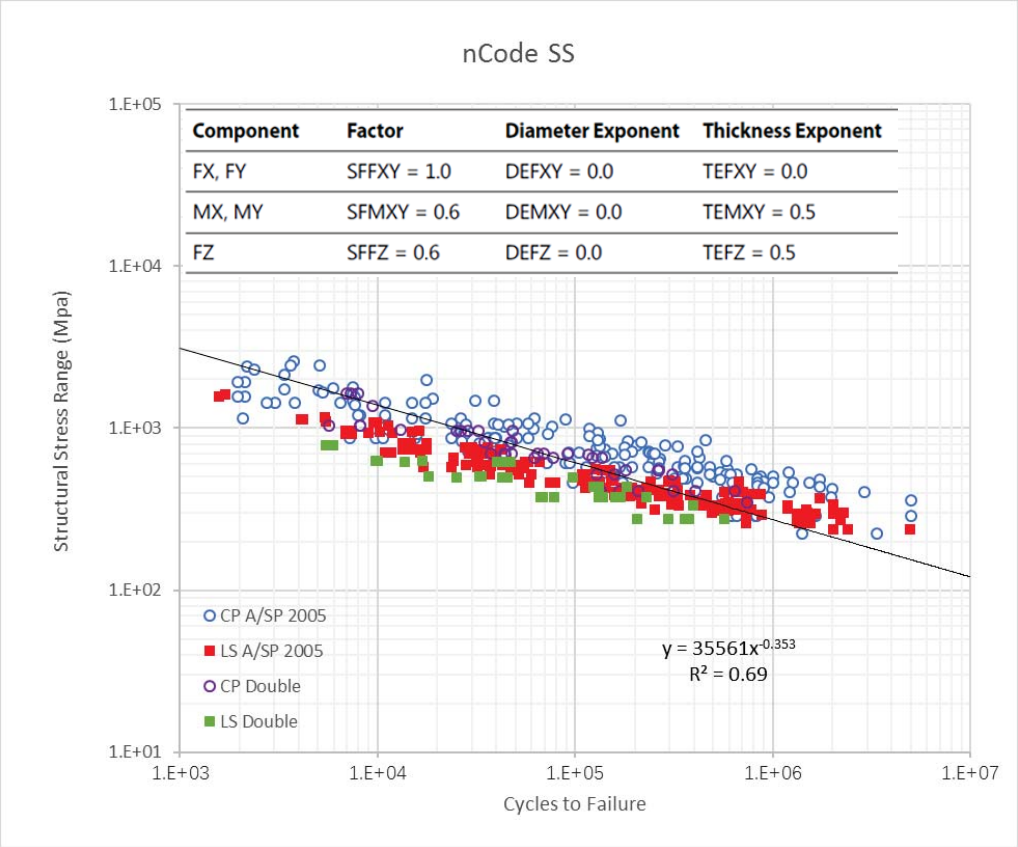

Figure 3.14. nCode structural stress range vs. cycles to failure for steel-steel

In nCode software material setting, ‘Generic Sheet’ was allocated to sheet material and ‘Generic Nugget' was assigned to spot weld nugget material. Therefore, Young's modulus for all the steel specimens was unified to 210 Gpa. The nine adjustable parameters were selected as the default value recommended by nCode as Fig 3.14. shows. According to above figure, a visible separation exists between coach peel and tensile-shear fatigue data (the coach peel curve runs above the tensile-shear curve). To collapse coach peel and tensile-shear data and reduce the scatters, a new set of nine parameters need to be created. Apparently, the new values of nine parameters strongly depend on the experimental fatigue data, which means that modifications have to be made each time for a new series testing data. Whereas the SCFs in notch stress method are definable based on the specimens’ dimensions.

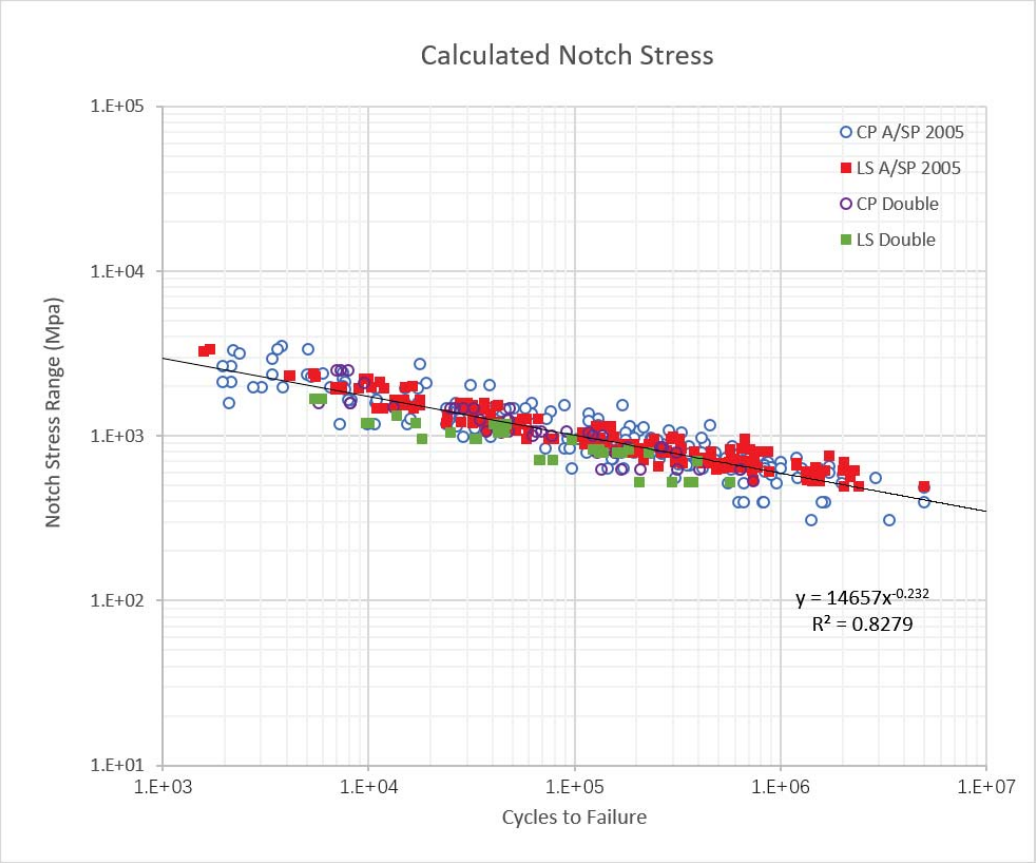

Figure 3.15. Notch stress range vs cycles to failure for steel-steel

A better collapsing fatigue data is shown in Fig 3.15. by notch stress method. Both scatters in different types of specimens (coach peel and tensile-shear) and within the same type of specimens are significantly reduced compared to nCode structural stress method (default value parameters).

3.5.2. Aluminum to Aluminum combination for spot-welded joints

In chapter II, historical fatigue data of Al to Al sheet combination for spot-welded joints were introduced to verify that whether the newly developed notch stress method is applicable for different sheet materials joints. First, fatigue data were processed with nCode Designlife software for comparison. The result is shown in Fig. 3.16.

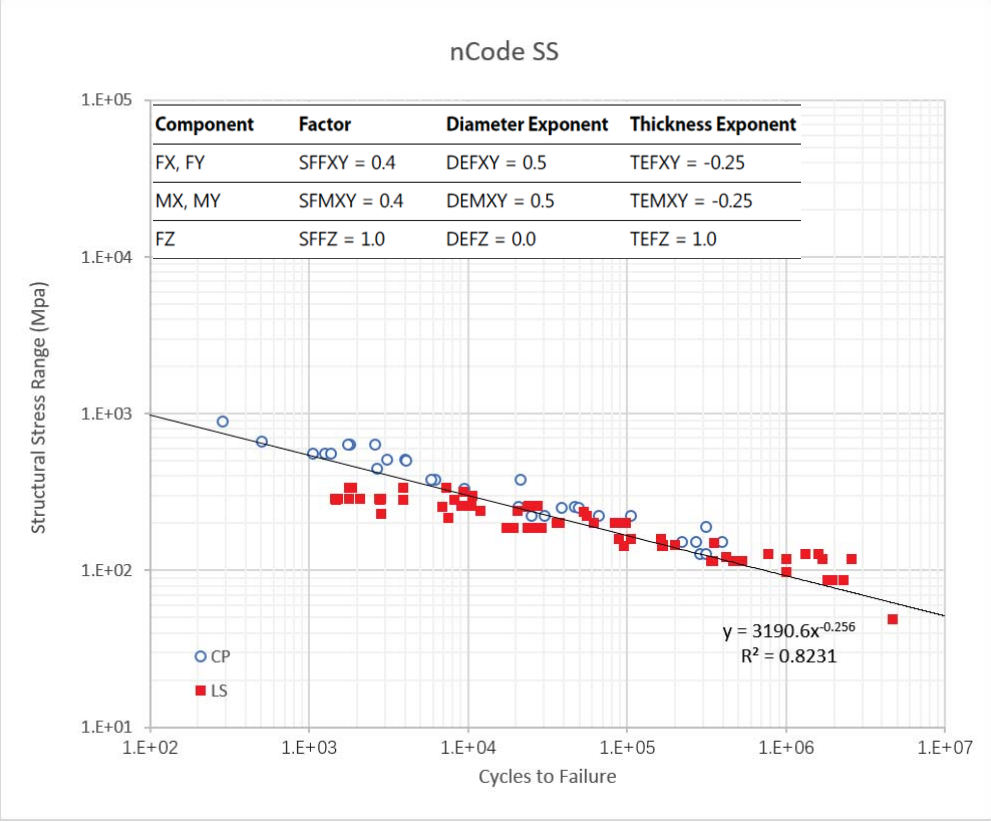

Figure 3.16. nCode structural stress range vs cycles to failure for Al-Al

In nCode software material setting, 'Al_Alloy_AlMg5Mn_Spot_Welds' was allocated to both sheet material and spot weld nugget material. Therefore, Young's modulus for all the steel specimens was unified to 70 Gpa. The nine adjustable parameters were selected as the default value recommended by nCode as Fig 3.16. shows. Note that theses nine parameters value were recommended by nCode manual [17]. After the parameters adjustment, the structural stress result reveals less scatter than steel to steel case in nCode method because the parameters of Al alloy are determined based on extensive existed experimental data. However, there is still slight separation between TS and CP in low cycles region (CP runs above TS).

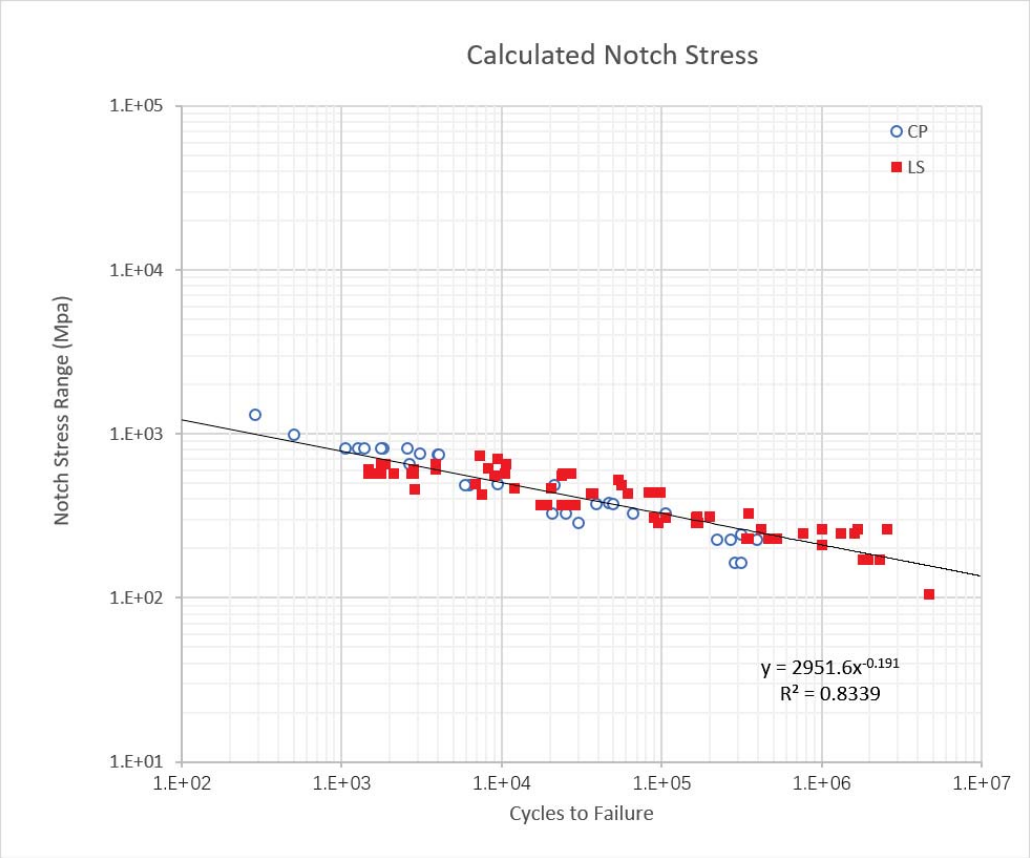

Figure 3.17. Notch stress range vs cycles to failure for Al-Al

Then, fatigue data were processed with notch stress calculation and the result is shown in Fig. 3.17. For TS specimens, the scatters have been reduced compared to the result from

nCode structural stress method. Also, in low cycles and middle cycles range, notch stress method reveal a better collapse for TS and CP.

3.5.3. Aluminum to steel combination for spot-welded joints

The particular group of dissimilar sheet materials spot weld specimens were analyzed in the same procedures as the other two groups. First, fatigue data were processed with nCode Designlife software. The result is shown in Fig 3.18.

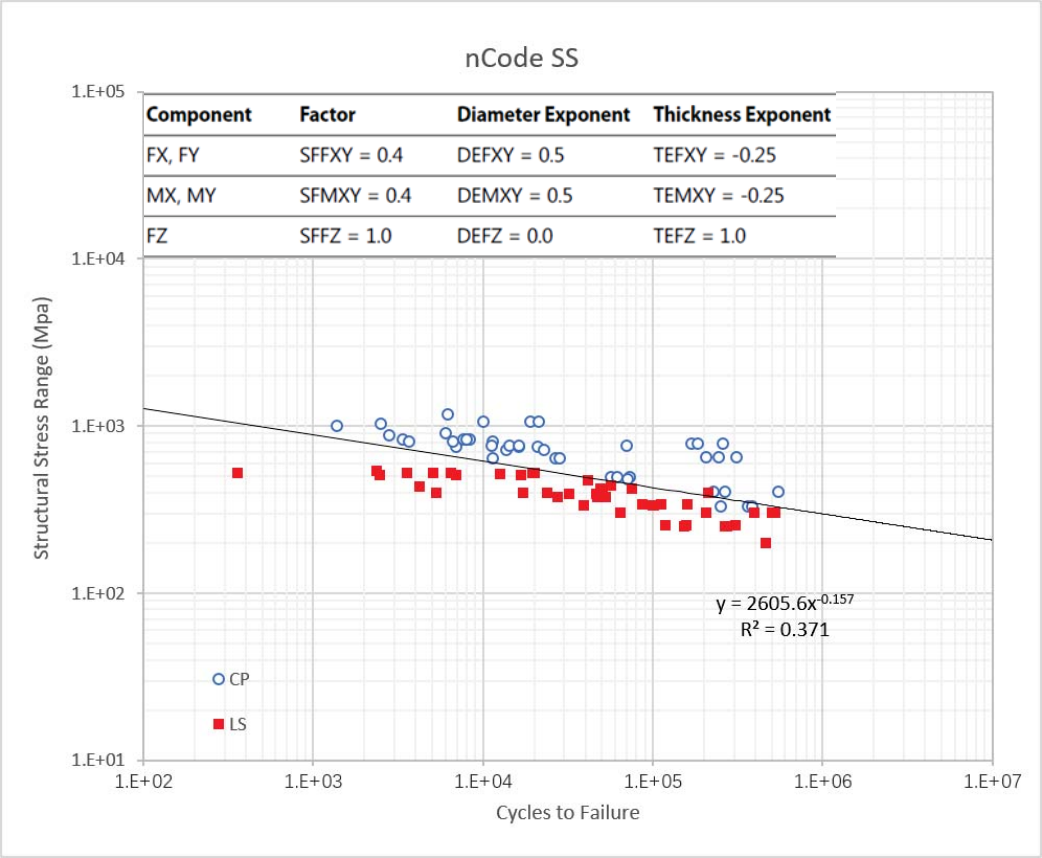

Figure 3.18. nCode structural stress range vs cycles to failure for Al-steel

In nCode Designlife software, there was no analysis engine for dissimilar sheet materials spot-welded joints. Therefore, the upper sheet was treated as aluminum alloy 'Al_Alloy_AlMg5Mn_Spot_Welds', the bottom sheet is dealt with as steel 'Generic Sheet, ' and spot weld nugget was selected as 'Generic Nugget,' which ensured that the stiffness of

nugget was large enough in analysis. The L-N curves for dissimilar materials combination were flatter than the similar material combination. Thus, the slope of S-N curves is smaller than other

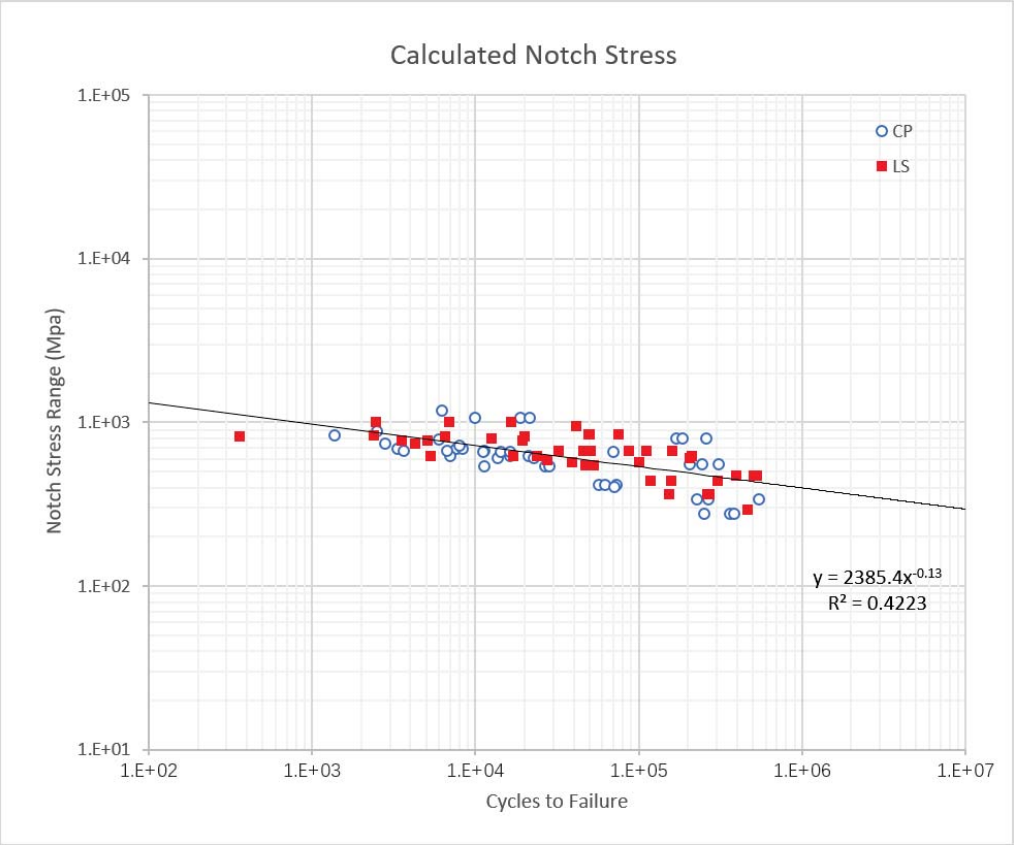

Figure 3.19. Notch stress range vs cycles to failure for Al-steel

two groups. Obviously, there is a large gap between CP data and TS data.

Then, fatigue data were processed with notch stress calculation and the result is shown in Fig. 3.19. CP and TS fatigue data can collapse. However, the apparent scatter still exists within similar geometric type of specimens. This phenomenon could imply that the thickness difference is the key factor accounting for the scatter. Finally, three groups of fatigue data are plotted together in Fig 3.20. There are two distinguishable S-N curves which are corresponding to steel to steel and Al to Al, respectively. Steel to steel S-N curve runs above Al to Al curve and Al to steel S-N curve lay between them as expected.

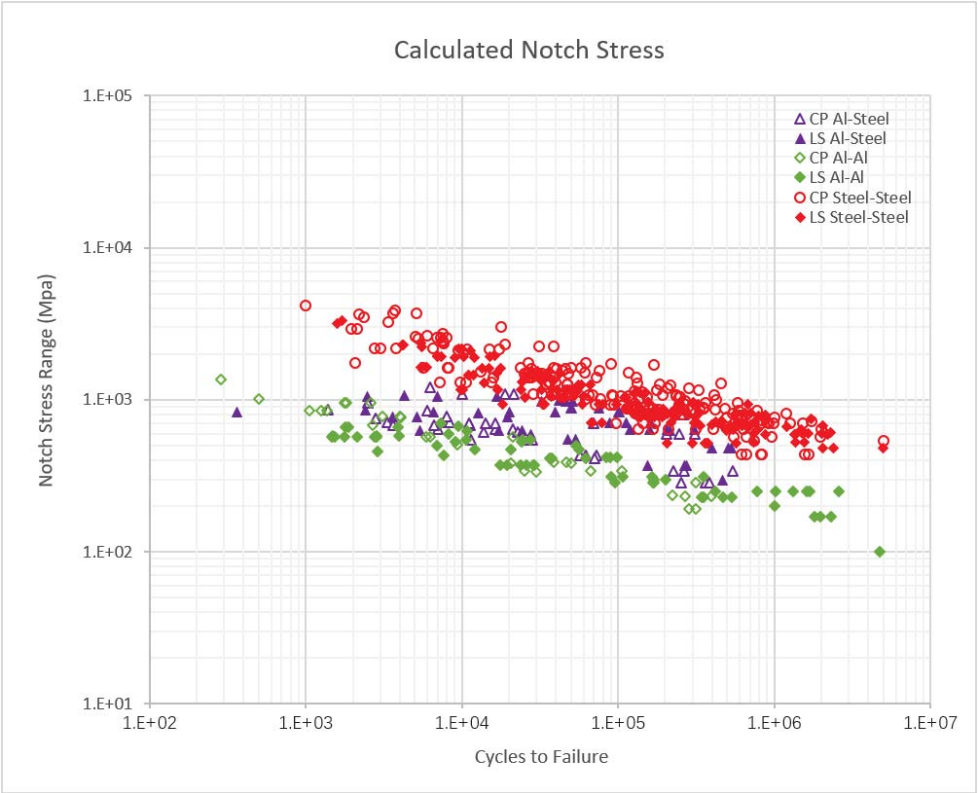

Figure 3.20. Notch stress range vs cycles to failure for all materials

References

[1] Radaj D, ‘Fatigue Assessment of Welded Joints by Local Approaches’ Abington Publishing, Cambridge, UK.

[2] Y. Zhang, D. Taylor, Sheet thickness effect of spot welds based on crack propagation, Engineering Fracture Mechanics 67 (2000) 55-63

[3] Pan N and Sheppard S D, ‘Spot welds fatigue life prediction with cyclic strain range’, Int J Fatigue, 2002, 24, 519–528.

[4] Zhang G and Richter B, ‘A new approach to the numerical fatigue-life prediction of spot-welded structures’, Fatigue Fract Engng Mater Struct, 2000, 23, 499–508.

[5] Seeger T, Greuling S, Brüning J, Leis P, Radaj D and Sonsino C M, Assessment of local concepts predicting the fatigue strength of spot-welded joints, FAT-Schriftenreihe 196, Frankfurt/M, FAT, 2005.

[6] Radaj D, Lehrke H P and Greuling S, ‘Theoretical fatigue-effective notch stresses at spot welds’, Fatigue Fract Engng Mater Struct, 2001, 24, 293–308.

[7] Zhang, S. Stress intensities derived from stresses around a spot weld. Int. J. Fract. 1999; 99: 239–257.

[8] Radaj, D. and Zhang, S. (1991a). Stress intensity factors for spot welds between plates of unequal thickness. Engineering Fracture Mechanics 39, 391–413.

[9] Zhang, S. Stress intensities at spot welds. Int. J. Fract. 1997; 88: 167–185.

[10] F. Erdogan and G. C. Sih (1963) On the crack extension in plates under plane loading and transverse shear. J. Basic Engng 85, 519–527.

[11] R. Yuuki, T. Ohira, H. Nakatsukasa and W. Yi (1985) Fracture mechanics analysis and evaluation of the fatigue strength of spot welded joints. Trans. Japan. Soc. Mech. Engrs. 51-467, 1772–1779.

[12] Rupp A, Störzel K and Grubisic V, ‘Computer-aided dimensioning of spotwelded automotive structures’, SAE Techn Paper 950711, Warrendale Pa, SAE, 1995.

[13] Nakahara, Y., Takahashi, M., Kawamoto, A., Fujimoto, M. et al. Method of Fatigue Life Estimation for Spot-Welded Structures SAE 2000-01-0779

[14] Lin, P.-C., Pan, J., 2008a. Closed-form structural stress and stress intensity factor solutions for spot welds in commonly used specimens. Engineering Fracture Mechanics, 45 (2008) 3996–4020

[15] Hong, J.K. Battelle. The development of a simplified spot weld model for Battelle structural stress calculation. SAE Technical Paper, 2011-01-0479

[16] Radaj D, Lehrke H P and Greuling S, 'Theoretical fatigue-effective notch stresses at spot welds', Fatigue Fract Engng Mater Struct, 2001, 24, 293–308.

[17] DesignLife Theory Guide: Spot Weld Analysis Engine NC-DL-TH 8.00.130

CHAPTER IV

CONCLUSION

In this thesis, some existing fatigue life evaluation methods for spot-welded joints were reviewed. Among them, Rupp's structural stress method was the simplest and widely used approach in the industry. However, there were some distinct weaknesses within structural stress method. First, there were nine parameters needed to be adjusted which ensured that the fatigue data can be correlated well. These nine parameters were solely determined based on large existing data source, which means that the nine parameters have to be updated each time when new experimental data are added to the data source. Second, the local effect such as notch effect of spot weld was completed neglected causing the accuracy decrease in evaluating stress distribution in the spot-welded joint. Last but not least, some self-balanced forces or moments could not be captured in structural stress approach. In chapter 2, three groups of fatigue data were presented including steel to steel sheet material combination, aluminum to aluminum sheet material combination and aluminum to steel mixed material combination. These three groups of fatigue data were first processed with nCode Designlife software using nCode default value for nine parameters. And the results were turned out to be bad. There was a distinct separation between tensile-shear (TS) and coach-peel (CP) S-N curves, which occurred in all three groups of fatigue data, especially in mixed material combination. Based on above observation, a new notch stress approach was developed in this study. Following conclusions

can be made on the advantages and improvement of this notch stress method.

1) The new notch stress approach introduced three stress concentration factors SCFs to eliminate the nine parameters which are merely based on curve fitting. The three nominal stresses corresponding to three SCFs are originated from Rupp's structural stress: membrane stress, bending stress from moments and bending stress due to opening force. It should be emphasized that the SCFs are determined on stress intensity factors SIFs in front of crack tip rather than geometric parameters of the spot weld. Moreover, SIFs can be calculated by the nominal normal stress distributed in plate sheet near spot weld nugget. This can be achieved by applying J-integral to a 2D plane cross-sectional model of the weld spot edge containing the slit tip.

2) The SCFs were calculated based on a 2D model. However, the commonly used spot weld model is established on 3D. Thus, in this study, some correction parameters are introduced to consider the effect of 3D boundary conditions.

3) The neglecting self-balanced force or moment in nCode structural stress method was taken into account in new notch stress approach. Generally speaking, the most accurate way to capture the self-balanced force or moment can be achieved by creating a high-density mesh around spot weld nugget periphery in FEA. Nevertheless, it was troublesome and time-consuming to be applied to every single spot-welded joint in the automotive industry, which approximately involved serval thousands of spot welds in a vehicle. Therefore, a simple assumption had been made in this study, which was that the relationship between self-balanced force and nodal force of nugget in general loading conditions was equal to the relationship in

simple specimens (TS and CP). Stress decomposition analysis can easily obtain the latter one. Once the output of nodal forces or moments in FEA is acquired, the self-balanced forces or moments can be determined.

4)The three groups of fatigue test results verified that the new notch stress approach revealed better correlation and less scatter than Rupp's structural stress method (nCode) with default parameters. However, some apparent scatter still existed within similar geometric type of specimens. And thickness difference was the key factor accounting for the scatter. Therefore, the thickness correction for spot-welded joint became a topic deserving to be discussed in the future study.